Catching targeting factors involved in co-translational import into mitochondria

Anna Engel

Major research internship

Molecular and Cellular Life Sciences

Examinator:
Prof. dr. F.G. Förster

Second Examinator:
Dr. A.I.P.M. de Kroon

Daily Supervisor:
L.M.K. Thärichen MSc

Structural Biochemistry, Department of Chemistry, Faculty of Science, Utrecht University

2021-12-24

Layman's Abstract

Cells within multicellular organisms have different compartments called organelles. One of these organelles is the mitochondrium, which provides the cell with the energy required to perform its functions. Most of the proteins within the mitochondria are brought there after they are synthesized by a molecular machine called the ribosome. This synthesis process is called translation. However, sometimes the proteins are also brought to the mitochondria while being translated, which is called co-translational targeting. Until now, co-translational targeting to the mitochondria has not been studied that well. In the yeast *S.cerevisiae,* it has been found that the nascent polypeptide-associated complex (NAC) interacts with actively translating ribosomes called ribosome nascent-chain complexes (RNCs). It is unknown if NAC has the same functions in mammals as in yeast. Moreover, there is hardly any structural information on the interaction between NAC and RNCs. This thesis aimed to find targeting factors like NAC in mammalian and yeast systems.

For this aim, a system that can translate the proteins is needed. This system is called an *in vitro* translation system. Therefore, a yeast *in vitro* translation system was established and optimized in the lab. To generate the RNCs, model proteins were chosen. The DNA of these model proteins was supplemented with a sequence that halts the translation by the ribosome to allow for the generation of RNCs. In addition, it contains a sequence that allows for the purification of the RNCs. The model proteins were then translated in the yeast *in vitro* and in a previously established mammalian *in vitro* translation system called rabbit reticulocyte lysate (RRL). The RNCs and empty ribosomes were isolated from the *in vitro* translation mixtures and imaged using negative stain electron microscopy (EM), which Is a technique that allow us to look at small molecules that we can not see with our eye. With this method, we could determine the sample homogeneity. The RRL RNCs were, but the yeast RNCs were not homogenous. Moreover, purification of the RNCs was attempted; however, this was unsuccessful.

Before we can find mitochondrial targeting factors, the purification of the RNCs needs to be optimized. When this is done, cryo-single particle analysis EM (cryo-SPA-EM) can be performed, which is a microscopy technique that allows us to look at molecules with higher detail than with negative stain EM. However, this also requires further optimization. Lastly, the newly established yeast *in vitro* translation system can be used for other applications such as research in other fields.

Abstract

Nuclear-encoded genes contain 99 % of the mitochondrial proteome. Proteins translated from these genes are targeted to the mitochondria before they are imported into the organelle. This targeting and import can occur post-translationally or co-translationally, of which the latter is not well described. In *S.cerevisiae,* there is evidence of proteins being co-translationally targeted through their N-terminal mitochondrial targeting sequence (MTS). Moreover, the nascent polypeptide-associated complex (NAC) has been shown to interact with ribosome nascent-chain complexes (RNCs). It has interaction partners on the mitochondrial membrane, suggesting it acts as a co-translational targeting chaperone. In mammals, there is also evidence of MTS-based co-translational import. However, it is unknown which targeting factors are involved. In addition, there is hardly any structural data available except for a cryo-single particle analysis (SPA) reconstruction of the *C.elegans* 60s ribosome-NAC complex. Therefore, this thesis aimed to find targeting factors like NAC in yeast and mammalian systems.

To find targeting factors in mammalian cells, OTC was chosen as a model protein since it was shown that the OTC MTS allows for co-translational import. OTC Truncations containing a CMV stalling peptide and an S1 aptamer were successfully translated in a rabbit reticulocyte lysate (RRL) *in vitro* translation system to generate stalled RNC complexes. The RNCs and ribosomes were successfully isolated from the RRL reaction mixture and imaged using negative stain electron microscopy (EM) and Cryo-EM, revealing aggregation of the generated RNCs. Moreover, affinity purification of the RNCs, using the S1 aptamer was attempted, which resulted in unspecific binding of the RNCs to the beads.

To study co-transitional import into the mitochondria in *S.cerevisiae,* a second *in vitro* translation system was successfully established and optimized in the lab. Moreover, this system successfully translated truncated MDH1, RNCs also containing a CMV stalling peptide and an S1 aptamer. The RNCs and ribosomes were successfully isolated from the yeast lysate in *vitro* reaction mixture and imaged using negative stain EM, revealing non-aggregating 80s *S.cerevisiae* ribosomes. Moreover, affinity purification of the RNCs, using the S1 aptamer was attempted, which resulted in unspecific binding of the RNCs to the beads.

.

Contents

1 Introduction

Mitochondria are organelles within eukaryotic cells that are responsible for many essential intracellular processes, such as oxidative phosphorylation and calcium signaling (Osellame et al., 2012). They contain approximately 1500 proteins, of which 99% are encoded by nuclear genes. These proteins are imported into the mitochondria through the mitochondrial import machinery (Dolezal, 2006; Neupert & Herrmann, 2007; Sickmann et al., 2003). This import machinery is an essential mechanism within mammalian cells, and dysfunction is linked to several pathologies such as cardiovascular disorders and neurodegenerative diseases (Palmer et al., 2021).

1.1 Mitochondrial protein import

Nuclear encoded preproteins targeted to the mitochondrial matrix (MM) are first imported through the translocase of the outer mitochondrial membrane (TOM) (**Figure 1**). The TOM complex consists of various proteins, of which a few are the receptors Tom20, Tom 22, and Tom70, and a general import pore called Tom40, which is the main component of the TOM complex. Tom20 and Tom70 are loosely associated with Tom40, whereas Tom22 is stably associated (Chacinska et al., 2009; Endo & Yamano, 2009; Neupert & Herrmann, 2007). MM targeted preproteins contain an N-terminal mitochondrial targeting presequence (MTS)(Chacinska et al., 2009; Endo & Yamano, 2009; Neupert & Herrmann, 2007), which is recognized by Tom22 and Tom20 (Abe et al., 2000; Backes et al., 2018; Yamamoto et al., 2009).

After translocation through Tom40, MM preproteins are further translocated from the inner membrane space (IMS) through the translocase of the inner mitochondrial membrane (TIM23), which is located in the inner membrane (IM) (Becker et al., 2019). The primary protein receptor of TIM23 is Tim50, which recognizes the MTS of proteins destined for the MM and facilitates the transfer from Tom40 to the TIM23 pore, Tim23 (Mokranjac et al., 2009; Schulz et al., 2011; Truscott et al., 2001; Yamamoto et al., 2002). Finally, after TIM23 mediated translocation, the MTS is cleaved by mitochondrial processing peptidase (MPP), which is located in the MM, resulting in a mature protein. (Fox, 2012; Taylor et al., 2001).

1.2 Post-translational targeting and import

Mitochondrial import of preproteins is preceded by a targeting step to the organelle (**figure 2A**). The majority of preproteins are targeted to the mitochondria post-translationally via a subset of chaperones, of which cytosolic Hsp70 is an essential one (Becker et al., 2019; Deshaies et al., 1988; Murakami et al., 1988; Sheffield et al., 1990; Terada et al., 1995). After binding to the preproteins, Hsp70 delivers them to Tom70 (Young et al., 2003). In mammals, targeting of the preproteins through Hsp70 is aided by Hsp90 (Bhangoo et al., 2007). Moreover, Hsp70 is aided by a subset of cochaperones that further stabilize the preprotein and potentially interact with Tom22 (Hoseini et al., 2016; Opaliński et al., 2018).

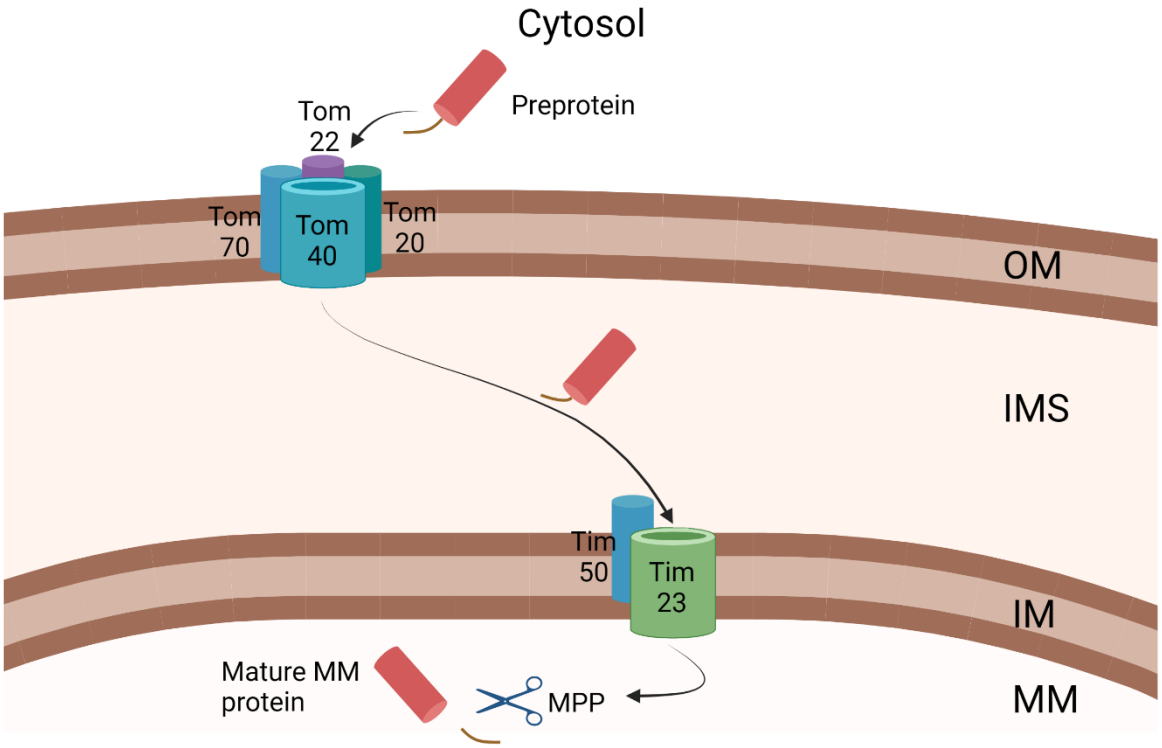

Figure 1. Mitochondrial protein import Schematic representation of protein import into the mitochondrial matrix (MM). Preproteins are translocated across the outer membrane (OM) through the translocase of the outer membrane (TOM) complex. From the inner membrane space (IMS), they are further translocated across the inner membrane (IM) by the translocase of the inner membrane (TIM) complex. After translocation into the MM, the mitochondrial targeting sequence (MTS) is cleaved off by mitochondrial processing peptidase (MPP).

1.3 Co-translational targeting and import

In addition to post-translational targeting, some preproteins can also be targeted and imported co-translationally. Co-translational targeting is not as well studied as post-translational targeting. However, several studies suggest that co-translational targeting is a common mechanism of preprotein targeting to the mitochondria.

In purified *S. cerevisiae* mitochondria, 80S ribosomes have been found to be isolated with them (Kellems & Butow, 1972). Additionally, fixed *S. cerevisiae* spheroplasts imaged using Electron Microscopy (EM) had ribosome-like particles situated at the OM, the endoplasmic reticulum (ER), and the outer nuclear membrane (Kellems et al., 1974). Of these ribosomes, two-thirds could only be released after adding the nascent chain releasing component puromycin, suggesting that the interaction between OM and ribosomes is nascent-chain dependent. These ribosomes are found mainly at specific regions of the OM close to the IM, suggesting that the ribosomes are located near protein import sites (Kellems et al., 1975). MRNA analysis of mitochondria-associated *S. cerevisiae* ribosomes revealed that most of these ribosomes predominantly translate mitochondrial proteins (Suissa & Schatz, 1982). When importing preproteins in a purely post-translational fashion, compared to a system where synthesis and import were allowed simultaneously, import of a COX4(1-12)-DFHR fusion protein was more efficient in the synthesis and import linked system (Fujiki & Verner, 1991). Moreover, inhibitors of post-translational import do not inhibit the import of COX4(1-22)-DHFR preproteins (Fujiki & Verner, 1993). Co-translational import is suggested to depend on the MTS since GFP with an ALDH-MTS is also imported in mitochondria of HeLa cells (Ni et al., 1999). A chimera of GFP with this N-terminal sequence and a C-terminal ER targeting sequence is exclusively found in the mitochondria, suggesting that the protein is already being targeted and imported before it is fully

translated. This same result was obtained in HeLa cells where the MTS of OTC allowed for the import of EGFP into mitochondria (Mukhopadhyay et al., 2004). Lastly, proximity-specific ribosome profiling of *S. cerevisiae* revealed that most IM proteins are translated at the mitochondrial surface, reminiscent of co-translational import into the ER (Williams et al., 2014). Collectively, these findings support the hypothesis that a subset of mitochondrial proteins can be imported co-translationally. There are two ways of co-translational targeting of nuclear-encoded preproteins via the 3'UTR or MTS targeting signals.

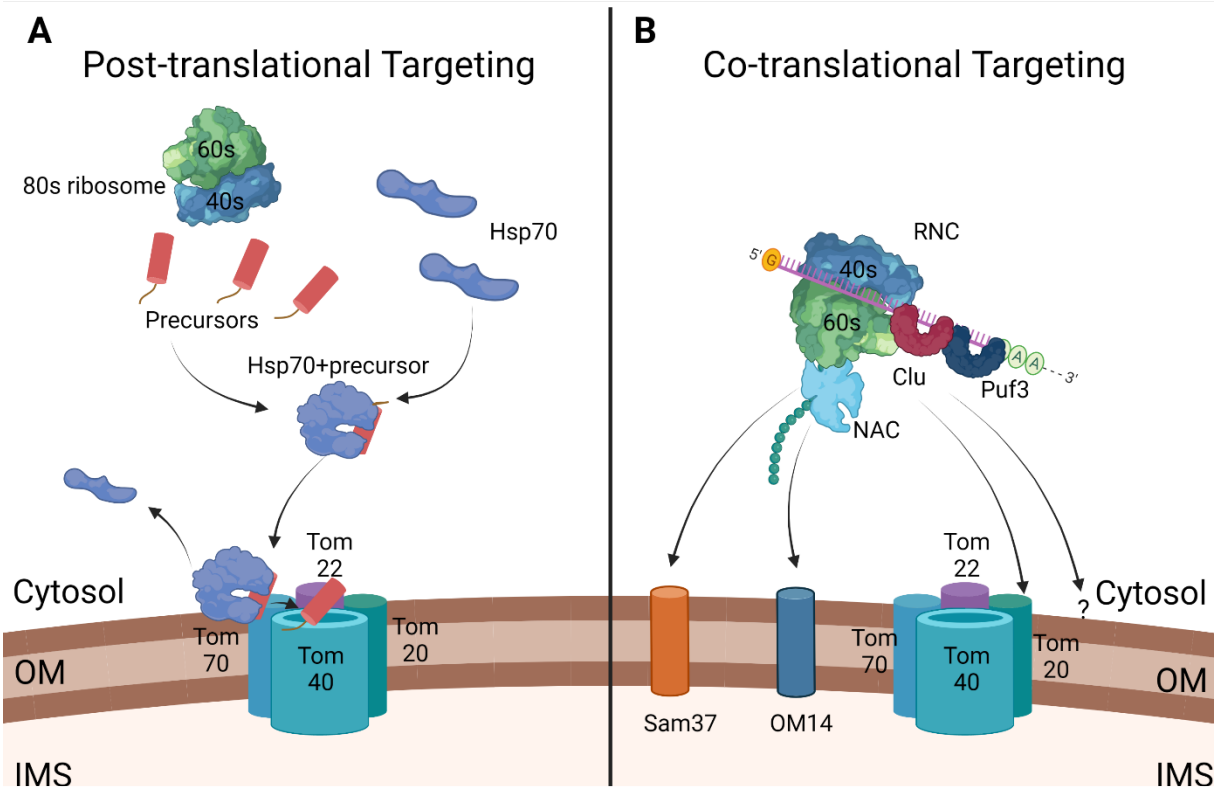

Figure 2. Post-translational versus co-translational targeting and import A) Schematic representation of post-translational targeting to mitochondria. After release from the translation machinery, proteins are handed over to Tom70 by Hsp70. **B)** Schematic representation of co-translational targeting to mitochondria. RNCs or nuclear-encoded mRNAs are guided to the OM via Clu and Puf3 interacting with the 3'UTR. RNCs can also be guided to the OM by NAC which has Sam37 and OM14 as interacting partners on the OM.

1.3.1 Targeting of mRNA to the mitochondria

As mentioned in the previous section, ribosome-nascent chain complexes (RNCs) can be targeted to the mitochondria through their mRNA, or they can be assembled onto the mRNA on the OM (**Figure 2B**). Research in *S. cerevisiae* showed that the 3'UTRs of mitochondrion-bound mRNAs on ribosomes contained sufficient information to target the ribosome to the OM (Marc et al., 2002). One of these 3'UTRs has subsequently been replaced by a 3'UTR of a cytosolic protein, resulting in reduced import of this protein into the mitochondria (Margeot et al., 2002). Affinity purification of the five mRNA binding Pumilio and FBF (PUF) family proteins showed that Puf3 nearly exclusively binds nuclear-encoded mRNAs (NEMs) (Gerber et al., 2004). (**Figure 2B**). In addition to Puf3, Clu was found to interact with NEMs and Tom20 (Sen et al., 2015; Sen & Cox, 2016). The human ortholog of Clu, called Cluh, has also been found to bind NEMs (Gao et al., 2014).

1.3.2 Targeting of ribosome-nascent chain complexes to the mitochondria

In addition to mRNA-mediated targeting, in *S.cerevisiae,* it has been observed that RNCs can be targeted to the mitochondria by an intermediate chaperone called nascent polypeptide-associated complex (NAC) (**Figure 2B)**. NAC can protect nascent chains in RNCs from interacting with other proteins in the cytosol and thus preventing aggregation (Wiedmann et al., 1994). NAC is present in the cell as a heterodimer consisting of an α-subunit and a β-subunit (Liu et al., 2010; Reimann et al., 1999). It acts as a general co-translational chaperone with subunits recognizing different features within nascent chains, thus suggesting it can have a wide range of nascent chain interactions targeted to different organelles such as the ER and the mitochondria (Alamo et al., 2011; Gamerdinger et al., 2015).

In an experiment where stalled RNCs containing MDH1 were generated and released from mitochondria by high salt concentrations, one of the significant factors released was NAC, showing that NAC interacts with RNCs (Fünfschilling & Rospert, 1999). The β-subunit binds in a salt-dependent manner to L23 ribosomal protein family members (Wegrzyn et al., 2006). Depletion of NAC results in defects in targeting RNCs to several locations, including the ER and mitochondria (George et al., 1998). Additionally, those cells have fewer ribosomes associated with the mitochondrial surface (George et al., 2002). In *S. cerevisiae*, the OM protein OM14 is one of the receptors for NAC. *OM14Δ* mitochondria show a significantly lower amount of associated NAC and ribosomes and decreased import efficiency of MDH1 *in vitro* (Lesnik et al., 2014). Another OM protein interacting with NAC is Sam37, which is part of the sorting and assembly machinery complex. Mutations in both NAC and Sam37 result in aggregation of Sod2 preproteins in the cytosol and have an altered mitochondrial protein content (Ponce-Rojas et al., 2017). Altogether, these results suggest a model of NAC guiding the RNC towards the mitochondrion where it interacts with OM14 and Sam37 in *S. cerevisiae.* Gamerdinger and co-workers obtained a cryo-SPA-EM reconstruction of a *C.elegans* 60S ribosome-NAC complex (**Figure S1**) (Gamerdinger et al., 2019). They were able to show that a subunit of NAC inserts itself into the ribosomal exit tunnel. In addition, a cross-linking experiment with mtHsp60 and NAC revealed that the shortest nascent chain found cross-linked to the β subunit had a length of 20 amino acids, suggesting that the β-subunit of NAC probes the ribosomal exit tunnel for MTS of nascent chains. The current hypothesis is that NAC positions itself at the ribosomal exit tunnel to inhibit the binding of other early targeting chaperones, Such as the signal recognition particle (SRP) and the ribosome-associated complex (RAC).

1.4 Research aims

Most of the scientific data on RNC targeting through NAC has been generated using *S.cerevisiae* translation systems; however, any structural data on the RNC-NAC complex is lacking. In mammals, the only data available is the 60s ribosome-NAC complex. However, scientific evidence of the role of NAC in mammals is missing. Therefore, this thesis aimed to catch targeting factors like NAC in *S.cerevisiae* and mammals using *in vitro* translation systems. In addition, we aimed to obtain an RNC-chaperone complex cryo-SPA-EM construction of *S.cerevisiae* and mammalian RNCs. For this aim, an *in vitro S.cerevisiae* translation system needs to be established. In addition, RNCs need to be generated in this *in vitro* translation system and in a rabbit reticulocyte lysate (RRL) *in vitro* translation system. As model proteins for *S.cerevisiae*, MDH1 and mtHsp60 will be used, and as a model protein for mammals, OTC will be used. After the RNC generation, RNCs will be purified using affinity purification. Cross-linking mass spectrometry needs to be performed to identify NAC or any other co-translational factors. Lastly, cryo-SPA-EM needs to be performed on purified RNCs to obtain a high-resolution reconstruction of an RNC-chaperone complex.

2 Materials and Methods

2.1 General chemicals

All general chemicals were purchased from Sigma Aldrich, Roche or Thermo Fisher Scientific if not noted otherwise.

2.2 Construction of plasmids

The plasmids (**Table S1**) were generated using polymerase chain reaction (PCR) based mutagenesis in a thermocycler S1000 (Bio-Rad) with a 25 µL volume with composition and amplification program as described in **Table 1** and **Table 2**. The annealing temperature used was based on the used primers' melting temperatures (T_m) as determined by SnapGene software (**Table S2**). To check for succesful amplification, 5µl of PCR product mixed with 1 µL 6x loading dye (NEB) was loaded on a 0.8% agarose gell with Sybr Safe (Invitrogen) in 1X TBE buffer and run for 45 minutes at 120 volts. DNA bands were imaged using UV light on a ChemiDoc XRS+ (Bio-Rad). Ligation of the PCR products was performed using enzyme KLD treatment as described in **Table 3**. The reaction was left at room temperature for 75 minutes and heat inactivated at 65°C for 5 minutes.

Table 1: PCR reaction plasmid

Components	**1 reaction (µL)**
10 ng/µl template	1
10 µM forward primer	1
10 µM reverse primer	1
10 mM dNTPS	1
5x Q5 buffer (NEB)	5
Q5 polymerase (NEB)	0.5
H_2O	15.5
Total volume	25

Table 2: PCR program

Temperature (°C)	**Time (s)**	
98	30	
98	10	25 cycles
~ T_m of primers	30	
72	90	
72	180	

Table 3: KLD treatment

Components	**1 reaction (µL)**
10x T4 ligase buffer (Thermo Scientific)	1
T4 ligase (Thermo Scientific)	0.2
T4 PN Kinase (NEB)	0.4
DpnI (NEB)	0.4
PEG 4K 50% (NEB)	0.5
PCR product	2
H_2O	5.5
Total volume	10

2.3 Transformation of competent *E.coli cells* and purification of plasmid DNA

The complete KLD reaction was added to 25 µl competent TOP10 *E.coli* cells from the TOP0 TA Cloning™ Kit (Invitrogen), incubated on ice for 20 minutes, and subsequently heatshocked for 45 seconds at 44°C after which 0.8 mL of LB was added and incubated at 37° for 45 minutes. After recovery, 150 µL of the mixture was plated on LB plates with corresponding antibiotics and left incubating overnight at 37°C. Colonies were picked and used for inoculation of 6 mL LB containing the corresponding antibiotics for each construct and left incubating overnight at 37°C. Plasmids were purified following the QIAprep Spin Miniprep Kit (QIAGEN), with the only adjustment being elution in 40 µl elution buffer.

2.4 Generation of *in vitro* translation template

DNA constructs were linearized using primers, as described in **Table S2**, following the PCR reaction protocol described in **Table 1** but with 50 µl volume. Three of these reactions were made per construct to generate a linear template with a > 300 ng/µl concentration. **Table 4** shows the PCR program that was used to generate these templates. Templates were subsequently purified using FavorPrep™ GEL/PCR Purification Kit (Favorgen) with an input of 140 µl PCR reaction and elution in 40 µl Nuclease-free water (Ambion). Templates with a concentration of >300 ng/µl were used as input for the *in vitro* transcription reactions.

Table 4: PCR program linear template generation

Temperature (°C)	**Time (s)**	
98	60	
98	20	
~ T_m of primers	30	35 cycles
72	30	
72	120	

2.5 In vitro transcription and mRNA purification

In vitro transcription (T1) was performed according to a protocol from the Hegde lab as described in (Sharma et al., 2010) (Established and optimized in the lab by dr. J. Fedry and Braakman & van der Sluijs lab). The transcription mixture (**Table 5**) was incubated at 37°C for 90 minutes in a cell culture water bath (Ecotemp TW20, Julabo) and then stored on ice. For analytical RRL reactions, one reaction of 5 µL was prepared. For other purposes (preparative RRL and yeast), 100 µL of reaction was prepared. From the 100 µL reactions, the mRNA was purified using an RNeasy Micro Kit (QIAGEN) using one purification column per linear template. Elution of the mRNA from the column was done using 40 µL Nuclease-free water (Ambion).

Table 5: Reaction mixture for *in vitro* transcription

Components	**Analytical reaction (µL)**	**Preparative reaction (µL)**
T1 mix buffer	3.8	76
RNAsin (Promega)	0.1	2
T7 Polymerase (NEB)	0.1	2
Linear template 300 ng/µL	1	20
Total	5	100

2.6 RRL *In vitro* translation

In vitro translation (T2) was performed according to a protocol from the Hegde lab as described in (Sharma et al., 2010) (Established and optimized in the lab by dr. J. Fedry and Braakman & van der Sluijs lab). The translation mixture (**Table 6**) was incubated at 30°C for 15 minutes in a water bath model 5M (Julabo) temperature regulated by the EC-BASIS temperature regulator (Julabo) and put on ice to terminate the reaction. For analytical reactions, a reaction volume of 5 µL was prepared and supplemented with 15 µl 2X SDS sample buffer for SDS-PAGE analysis. For preparative reactions, four times 100 µL was prepared.

Table 6: Reaction mixture for *in vitro* translation RRL

Component	Analytical reaction (µL)	Preparative reaction (µL)
T2 mix	2.5	50
Nuclease-free water (Ambion)	2	26
[^{35}S]-L-Met and [^{35}S]-L-Cys 11mCi/mL (PerkinElmer)	0.25	/
Unlabeled Met en Cys, 1.75 mM	/	5
Purified mRNA 350 ng/uL	0.5	19
Total	5	100

2.7 Autoradiography

7 µl of the RRL analytical reaction was loaded on a 15% SDS-PAGE gel (resolving gel: 1.1 mL H_2O, 2.5 mL 30% acrylamide mix, 1.3 mL 1.5 M Tris pH 8.8, 0.05 mL 10% SDS, 0.05 mL 10% APS, 0.002 mL TEMED. Stacking gel: 0.68 mL H_2O, 0.17 mL 30% acrylamide mix, 0.13mL 1.0 M Tris pH 6.8, 0.01 mL 10% SDS, 0.01 mL 10% APS, 0.001 mL TEMED). The gel was run at 25 mA for 50 minutes and then fixed in 20% methanol and 10% acetic acid for 30-45 minutes. The gel was subsequently dried onto paper for 1 hour and put into a cassette with erased phosphor film (GE Healthcare) to expose overnight. The SDS-PAGE gel was then imaged in a Typhoon™ FLA 7000 (GE Healthcare) using the 800 PMT amplification setting.

2.8 Yeast in vitro translation

2 L of YPD medium for the *S.cerevisiae* strain S288C was inoculated to an OD600 of 0.001 and grown for 16-20 hours at 30° and 150 rpm. Cells were then harvested at OD600 of 1.5 by centrifugation for 8 minutes at 4000 rpm at room temperature. The pellets were resuspended in 400 mL 1xPBS and then centrifuged for 5 minutes. The pellets were then resuspended in 25 mL cold autoclaved water, transferred to a pre-weighted 50 mL falcon tube, and filled up to 50 mL with cold autoclaved water. After centrifugation for 4 minutes, the pellet was resuspended in 5mL 10% Glycerol in MilliQ per 15 gram and subsequently frozen as droplets in liquid nitrogen. Cells were lysed by cryo-milling in the TissueLyser II (Retsch) twice for 1 minute at 30 hertz and stored in -80°C.

4 grams of yeast powder were thawed and resuspended on ice in 1.6 mL ice-cold sterile buffer A (30mM Hepes pH 7.5, 100mM KOAc pH 7.0, 3mM $Mg(OAc)_2$, 2mM DTT, 0.5mM PMSF), transferred to five 1.5 mL microcentrifuge tubes, and then centrifuged at 4°C for 10 minutes at 17000 rpm. The supernatant was transferred to fresh tubes and again centrifuged. The supernatant was then loaded onto a pre-equilibrated PD10 desalting column (GE Healthcare) and eluted with 3.5 mL buffer A while collecting ~ 300µL fractions. The OD260 of the fractions were measured (1 OD260 = 20nM), and fractions with OD260 > 100 were combined. Total yeast lysate was then treated with Micrococcal nuclease (NEB) at 15 U/ml and 0.75mM $CaCl_2$ for 7 minutes at 25°C. The treatment was inactivated by adding 3mM EGTA, and the extract was frozen as 50 µL aliquots in liquid nitrogen and stored at -80°C.

10X buffer B (15.6mM ATP, 2.5mM GTP, 160mM creatine phosphate, 4.5 mg/mL creatine kinase, 500 µg/mL t-RNA (brewers yeast), 4mM Spermidine) was prepared on ice by dissolving 2.25 mg of creatine kinase in 381.5 µL 5mM Hepes pH 7.5. Other components except creatine phosphate were added up until 500 µL, 29.5 mg creatine kinase was then dissolved in the mixture and the mixture was frozen as 20µL aliquots in liquid nitrogen and stored at -80°C. 2.5 mM Amino acid stock was prepared by weighing individual amino acids for a 500µl 100mM stock in 5M KOH and then adjusted to pH 7 by addition of 10M HCl. This high concentration of amino acids caused precipitation, therefore the amino acid stock was diluted to a 2.5 mM stock with pH 7.

Yeast lysate extract, 10X buffer B, 10X buffer A (140mM Hepes pH 7.5, 750mM KOAc, 12.5mM $Mg(OAc)_2$, 20mM DTT), 2.5 mM Amino acid mix, and RNAse inhibitor (Promega) were mixed as shown in **Table 7**. 10X buffer B and the Yeast lysate extract were slowly thawed on ice before they were added to the mixture. The translation mixture was added to the purified mRNA, properly mixed, and then incubated in a water bath model 5M (Julabo) temperature regulated by the EC-BASIS temperature regulator (Julabo) for 50 minutes at 20°C. The reaction was terminated by adding 0.2 mg/ml cycloheximide and subsequently put on ice. For analytical reactions, 20 µL of reaction was prepared and supplemented with 10 µl 3X SDS sample buffer for SDS-PAGE analysis. For preparative reactions, two times 100 µL reactions were prepared.

Table 7 Reaction mixture for *in vitro* translation yeast

Component	Analytical reaction (µL)	Preparative reaction (µL)
mRNA 250 ng/µL	3.9	19.5
10X Buffer B	2	10
10X Buffer A	2	10
Amino acid Mix 250 µM	2	10
RNAse inhibitor (Promega)	0.1	0.5
Yeast lysate extract	10	50
Total	20	100

2.9 RNC and ribosome isolation

The translation reaction, for both the RRL (400 µL) and yeast lysate (200 µL) preparative *in vitro* translation reactions, were loaded onto a 600µL ice-cold sucrose cushion (50mM Hepes pH 7.4, 100mM NaCl/NaOAc, 25mM $MgCl_2$/$Mg(OAc)_2$, 1mM DTT, 1M Sucrose) and ultracentrifuged in an Optima TL ultracentrifuge (Beckman) for 75 minutes at 4°C and 350 000 g (95 000 rpm) in a TLA100.2 rotor using 2 mL polycarbonate thick wall tubes (Beckmann). The supernatant was carefully pipetted off and the ribosome pellet was resuspended in 10 µl RNC buffer (50mM Hepes pH7.4, 50mM NaCl/NaOAc, 10mM $MgCl_2$/$MG(OAc)_2$, 0.4 U/µl RNAsin (Promega), 1mM DTT) if the pellet was used for western blot analysis (Section 2.11). The ribosome pellet was resuspended in 300 µl binding buffer (20mM Hepes pH 7.4, 150 mM NaCl/NaOAc, 20 mM $MgCl_2$/$Mg(OAc)_2$, 2mM DTT, 0.2 U/µl RNAsin (Promega), 1 tablet/50 mL cOmplete™, mini, EDTA-free Protease Inhibitor Cocktail (Roche)) if the pellet was used for affinity purification (Section 2.10). RRL ribosome pellet was resuspended in RNC buffer to 40 between 50 nM and yeast lysate ribosome pellet was resuspended in RNC buffer to 70 between 80 nM RNC buffer for negative stain-EM (section 2.12.1). For Cryo- EM (section 2.12.2) RRL ribosome pellets we resuspended in 20 µl RNC buffer and resuspended using a glass tube and a shaker for 30 minutes at 4°C. The sample was then centrifuged for 10 minutes at 17 000 rpm at 4°C. The supernatant was measured and further dissolved in RNC buffer to an OD260 of 4 mAU

2.10 RNC affinity purification

50 µl of Pierce Streptavidin Magnetic Beads (Thermo Scientific) were washed twice with 1 mL washing buffer (20mM Hepes pH 7.4, 150 mM NaCl/NaOAc, 20 mM $MgCl_2$/$Mg(OAc)_2$, 2mM DTT). 300µl of ribosome pellet was incubated on the beads for 1 hour at 4°C under rotation. Beads were then washed twice with 300 µl washing buffer and afterwards incubated for 1 hour at 4°C under rotation in binding buffer supplemented with 5mM Biotin. Supernatant was saved after each step and beads were afterwards cooked with 100 µL 3x SDS sample buffer for 5 minutes at 96°C. 0.11 volumes of ice-cold 100% TCA was added to supernatant and then placed on ice for 10 minutes. Subsequently 500 µl of ice-cold 10% TCA was added to the sample, left on ice for 20 minutes, and centrifuged for 30 minutes at 4°C and 20 000 x g. The supernatant was removed and pellets were washed using 500 µl acetone and centrifuged for 10 minutes at 4°C and 20 000 x g. Protein pellets were dried in a flowcabinet for 5-10 minutes and then resuspended in 10 µl RNC buffer and 5 µl 3x SDS sample buffer.

2.11 Western blot analysis

10 µl sample was loaded onto 12% or 4-15 gradient % Mini-PROTEAN© TGX™ Precasted Gels (Bio-Rad) and run for 50 minutes at 120 volts. The protein bands were transferred using a premade Trans-Blot Turbo Transfer PVDF membrane (Bio-Rad) and the mixed MW setting on the Trans-Blot Turbo Transfer System (Bio-Rad) was used. The membrane was blocked in a 5 % milk PBS solution for 1 hour at room temperature. The membrane was then incubated with primary antibody in 5% milk PBS containing 0.005% Tween-20 solution (mouse Anti-Flag M2 Monoclonal antibody 1:2000, F1804 Sigma Aldrich) for 4 hours at room temperature or overnight at 4°C. Membrane was then washed for 5, 10, and 15 minutes in PBST before being incubated for 1 hour at roomtemperature in 5% Milk PBST containing secondary antibody (Goat Anti-Mouse Poly-HRP 1:3000, 32230 Invitrogen). The membrane was then washed again for 5, 10, and 15 minutes in PBST. The blot was then developed using 500 µl Amersham ECL Detection Reagents (Cytiva) and imaged using chemiluminesence on a ChemiDoc XRS+ (Bio-Rad). exposing for 1-10 minutes every minute.

2.12 Electron microscopy

2.12.1 Negative stain

Cu 400 (100) Carbon film grids were glow discharged before 4µl of 40-50 nM rabbit RNC or 70-80 nM yeast RNC solution was pipetted on the grid and immediately blotted off using Whatman No. 1 blotting paper. The grid was washed three times using MilliQ water, stained 3 times 10s with spun down 2x Uranyl acetate and then air dried. Grids were imaged using a TALOS L120C TEM (Thermo Fisher Scientific), with a 4k x 4k Ceta CMOS camera (Thermo Fisher Scientific) at 73 000 x magnifications resulting in a pixel size of 1.95 Å.

2.12.2 Cryo-EM

Quantifoil Holey R 2/1 Cu 200 grids were glow discharged before 4 µ of RRL RNC sample at an OD260 of 4 mAU was pipetted on the grid and immediately blotted of for 4.0 seconds with a blot force of 0 in the vitrobot II (Thermo Fisher Scientific). The sample was then plunge frozen in liquid ethane and transferred to liquid nitrogen. Grids were mounted into autogrid cartridges and imaged using TALOS Arctica at 200kV with a Gatan energy filter and a K2 summit camera (Thermo Fisher Scientific) equipped with Gatan energy filter at 6 000 x and 130 000 x magnifications resulting in a pixel size of 24.16 Å and 1.041 Å, respectively.

2.13 Schematic figures

Schematic figures were created with BioRender.com

3 Results

3.1 Construct generation for *in vitro* translation in RRL and yeast lysate

To probe for factors involved in co-translational mitochondrial import in mammals and yeast, model proteins are required that can induce stalling in the ribosome and can be purified using affinity purification. To this end, constructs were generated containing a CMV stalling peptide (**Figure 3A & Table S1, constructs 70,112-113**). A double FLAG tag was added to detect the model proteins in western blot analysis. This tag cannot be used for affinity purification since it will be inside the ribosomal exit tunnel and is not accessible for pulldown (Dao Duc et al., 2019). Therefore, an S1 RNA aptamer was added to the 3'UTR, which can be used for purification using streptavidin beads (Leppek & Stoecklin, 2014).

After adding these components to the construct, truncations of the proteins were generated to allow for probing along the nascent chains when the RNCs are generated. (**Figure 3B & Table S1, constructs 84-89,117-130**). In addition, one OTC template of construct 89 was generated by using a reverse primer that limits the length of the nascent chain to 20 amino acids consisting purely of the MTS. As previously explained, NAC can sense the nascent chain in an RNC when it is 20 amino acids long (Gamerdinger et al., 2019). Therefore it is also worthwhile to test this small 20 amino acid long template. Due to this length constriction, the nascent chain does not contain a 2xFLAG tag or a CMV stalling peptide but will induce stalling based on previous research showing that an mRNA lacking a stop codon also stalls the ribosome (MacKenzie & Payne, 2004).

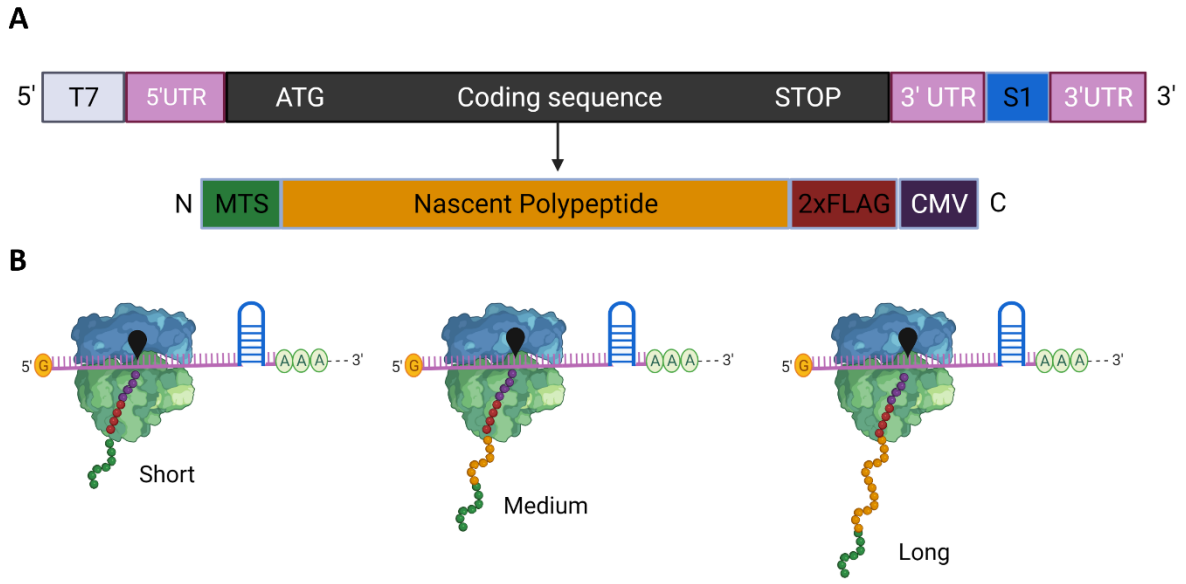

Figure 3. Construct design for RNC generation *in vitro* A) Schematic representation of constructs containing a CMV stalling peptide, a double FLAG, and a S1 RNA aptamer. **B)** Schematic representation of generated RNCs**.** CMV in purple, 2xFLAG tag in red, S1 aptamer in blue, peptidyl-tRNA in yellow, nascent chain in orange, and MTS in green.

3.2 *in vitro* translation and RNC generation in RRL

RNCs presenting a mammalian model protein were required to study mammalian co-translational import into mitochondria. To this end, OTC was used as a model protein in RRL *in vitro* translation to generate RRL-derived RNCs.

3.2.1 The RRL *in vitro* translation system can efficiently translate OTC model proteins

All constructs were transcribed using an already established and optimized *in vitro* transcription system (**Section 2.5**). After transcription, mRNA was purified and subsequently used as input for *in vitro* translation reactions (**Section 2.6**). The *in vitro* translation reactions were performed using radiolabeled [^{35}S] methionine and cysteine and were subsequently analyzed using autoradiography (**Figure 4A**). On the SDS-PAGE gel, the peptidyl-tRNAs migrate with a size between ~25 and ~37 kDa and the nascent chains between ~10 and 15 kDa. All constructs except for OTC20 were expressed. The ratio between stalled RNCs and nascent chain reveals a higher amount of stalled ribosomes than released nascent chain present, indicating that the stalling of the CMV peptide is efficient.

To express the OTC 20 construct, the corresponding DNA template was prepared using different approaches by adjusting the PCR program or using ethanol precipitation as a purification method after the PCR reaction. Moreover, the DNA template was prepared from different plasmids (**Table S1 constructs 84-89)**. These different approaches did not result in significant expression in RRL, and the construct was therefore not pursued any further.

For the OTC 32 and 82 *in vitro* translation reactions, RNCs/ribosomes were isolated by ultracentrifugation through a 1M sucrose cushion (**Figure 4B**). Western blot imaging using the FLAG tag in these isolated ribosome samples showed that the ribosome cushion separates the stalled ribosomes from the free nascent chains. To validate if 80s ribosomes are present in the sample, negative stain EM was performed (**Figure 4C & D**). The ribosomes are not homogeneously distributed, and they aggregate in the OTC 82 sample, but less so in the OTC 32 sample. In addition, minor contaminating particles can be seen in the OTC 32 and OTC 82 samples, which are most likely co-sedimenting proteasomes (**Figure 4C & D**).

The ratio between empty ribosomes and RNCs cannot be deduced from these images; therefore, grids for cryo-SPA-EM were screened. Isolated ribosomes (**Figure S2A**) were imaged under cryogenic conditions on a Cu 300 Quantifoil R2/2 grid with an additional 4 nm carbon film. Medium magnification images of these grids show that the ribosomes are not homogeneously distributed in the ice (**Figure S2B**). High magnification images reveal large aggregated clusters of ribosomes (**Figure S2C**), similar to the negative stain images of the same sample (**Figure 4C**). Of note, a different buffer, lacking salt and DTT, was used to resolubilize the ribosomal pellet, then described in section 2.9.

Therefore, to improve the distribution on the grid and reduce aggregation, the pellets obtained after ribosome isolation were additionally resuspended in RNC buffer for 30 minutes using a glass tube and shaker. Lastly, the sample was centrifuged for 10 minutes at 17 000 g to remove large aggregates. In addition, to sample preparation adjustments, the sample was imaged on a Cu 200 Quantifoil R2/1 grid without additional carbon (**Figure S2D**). At high magnification, the amount of aggregation does not seem less; however, there are slightly more particles in the ice for this type of grid (Data not shown).

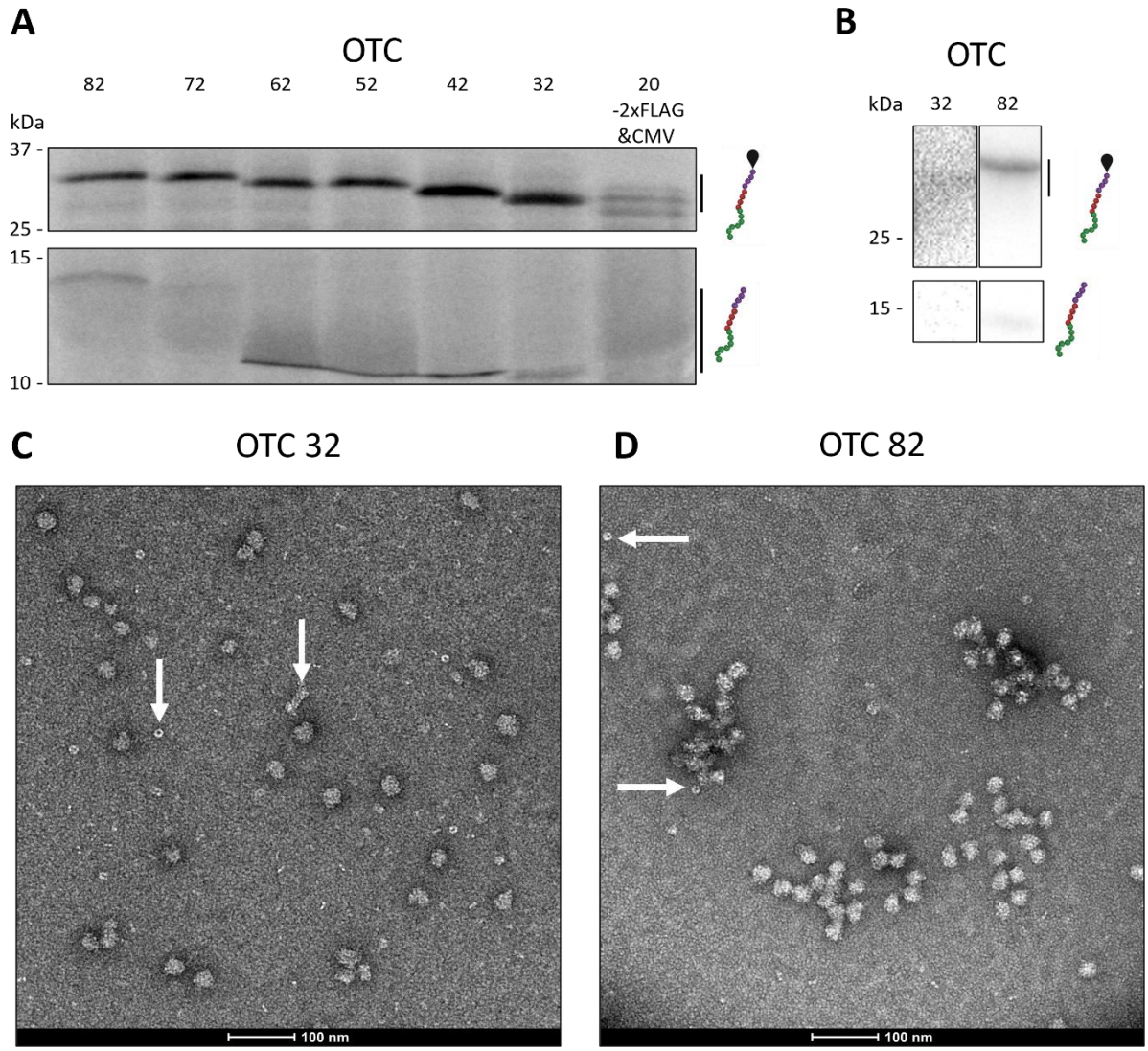

Figure 4. ***In vitro*** **translation and ribosome isolation A)** Autoradiography analysis of *in vitro* translation reactions of OTC truncations**. B)** anti-FLAG tag western blot of OTC 32 and OTC 82 ribosome pellets after *in vitro* translation and ultracentrifugation. **C)** Negative stain EM image at 73 000 x magnification of the OTC 32 RNC/ribosome sample at 40 nM concentration. White arrows indicate impurities in the sample. **D)** Negative stain EM image at 73 000 x magnification of the OTC 82 RNC/ribosome sample at 40 nM concentration. White arrows indicate impurities in the sample. (Upper cartoon signifies peptidyl-tRNA nascent chain and lower cartoon signifies free nascent chain).

3.2.2 Affinity purification of RNCs from RRL

To isolate RNCs, affinity purification was attempted. 400 µl *in vitro* translation reaction was ultracentrifuged, the RNC/ribosome pellet was resolubilized in 300 µl bead compatible binding buffer, and pulled down using 50 µl beads (**Figure 5A**). Western blot analysis reveals that the input signal (**Figure 5B lane 1**) is very low on the gel, in addition to there being no signal in the flowthrough, washing, beads before elution, and elution steps (**Figure 5B lanes 2-6**). The RNCs are bound to the beads unspecifically (**Figure 5B lane 7)** since elution with biotin did not release the RNCs. In addition, the majority of the RNCs in this fraction run lower on the gel than expected, and two RNC bands are present. An affinity pulldown of the construct lacking the S1 aptamer confirms the unspecific binding of the RNCs to the beads. (**Figure 5C lanes 5-7**).

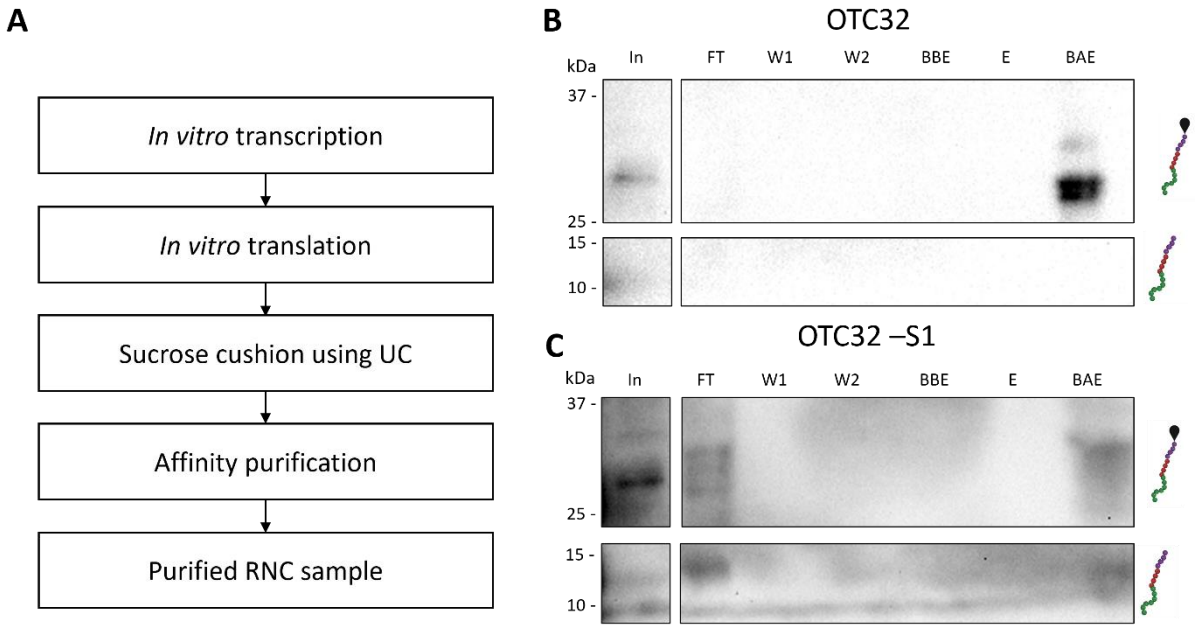

Figure 5. Affinity purification of OTC 32 RNCs A) RNC purification protocol (UC: Ultracentrifugation) **B)** Anti-FLAG western blot of the RNC pulldown experiment for the OTC 32 construct via the S1 aptamer **C)** Anti-FLAG western blot of the RNC pulldown experiment for the OTC 32 construct lacking the S1 aptamer. (In: Input, FT: Flowthrough, W1: Wash 1, W2: Wash 2, BBE: Beads before elution, E: Elution, BAE: Beads after elution) (Upper cartoon signifies peptidyl-tRNA nascent chain and lower cartoon signifies free nascent chain).

3.3 in vitro translation and RNC purification in yeast lysate

To generate RNCs for yeast proteins, an optimized yeast *in vitro* translation system was established and optimized using MDH1 and mtHsp60 as model proteins. Additionally, truncated MDH1 constructs were used to generate yeast-derived RNCs.

3.3.1 Establishing and optimization of a yeast *in vitro* translation system

A yeast lysate *in vitro* translation system was established as described in section 2.8 with wildtype S288C *S.cerevisiae* yeast strain (**figure 6A**). The yeast lysate OD260 values were measured, and fractions higher than 100 mAU were combined while fractions lower than 100 mAU were discarded, resulting in a yeast lysate with an OD260 of ~108 mAU (**figure 6B**).

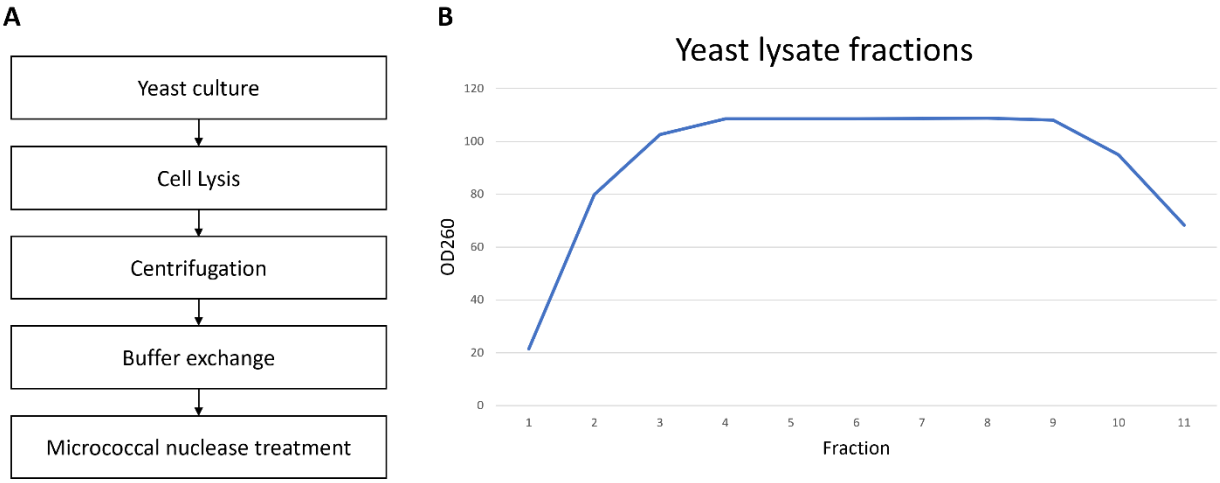

Figure 6 Yeast lysate extract preparation A) Yeast extract preparation workflow. **B)** OD260 measurements of yeast lysate fractions after buffer exchange.

The *in vitro* translation reaction conditions were optimized to obtain efficient expression. Optimization trials were performed using the first 186 amino acids of mtHsp60 and were analyzed by western blot using the double FLAG tag present in the construct. On the SDS-PAGE gel, the peptidyl-tRNAs migrate with a size between ~37 and ~50 kDa and the nascent chains between ~20 and 25 kDa (**Figure 7A**). At 70 minutes of translation (**Figure 7A lane 2**), the amount of translation product seems the highest, decreasing with a longer translation time (**Figure 7A lanes 3-7**). The amount of product does not significantly differ between 50 and 70 minutes (**Figure 7B lanes 1, 3, and 5**), nor does it differ for mRNA input concentrations higher than 250 ng/µl (**Figure 7B lanes 2, 4, and 6**). Therefore, 50 minutes of translation time with 250 ng/µl mRNA input concentration were chosen for further translation reactions.

Another critical parameter was the concentration of RNase inhibitor since this has been shown to inhibit translation reactions at a high concentration (Earl et al., 2018). A concentration of 0.4 U/µl already inhibits the translation reaction (**Figure 7C lanes 2 and 3**), while 0.2 U/µl did not (**Figure 7C lanes 5 and 6**) and, therefore, a concentration of 0.2 U/µl was used in further translation experiments. Lastly, the optimal temperature for the reaction was determined using constructs containing amino acids 1-94 of mtHsp60 or MDH1, respectively. In this experiment, a temperature of 20 °C (**Figure 7, lanes 1 and 2**) shows a higher amount of translation and ribosome stalling than at 25 °C (**Figure 7D lanes 3 and 4**). 20 °C was therefore chosen for further translation experiments.

In all the optimization experiments, there is a signal for two species of nascent chain, and sometimes even three (**Figure 7B lane 6, 7C lane 6 and 7D lanes 1-4**), since there is only signal for one species of peptidyl-tRNA, this is not deemed problematic. Lastly, the optimizations based on Hsp60 RNCs were applied to three different MDH1 truncations (**Figure 7E**). For all truncations, translation, as well as ribosome stalling, is observed. However, additional bands are present for the peptidyl t-RNA signal and the free nascent chain signal.

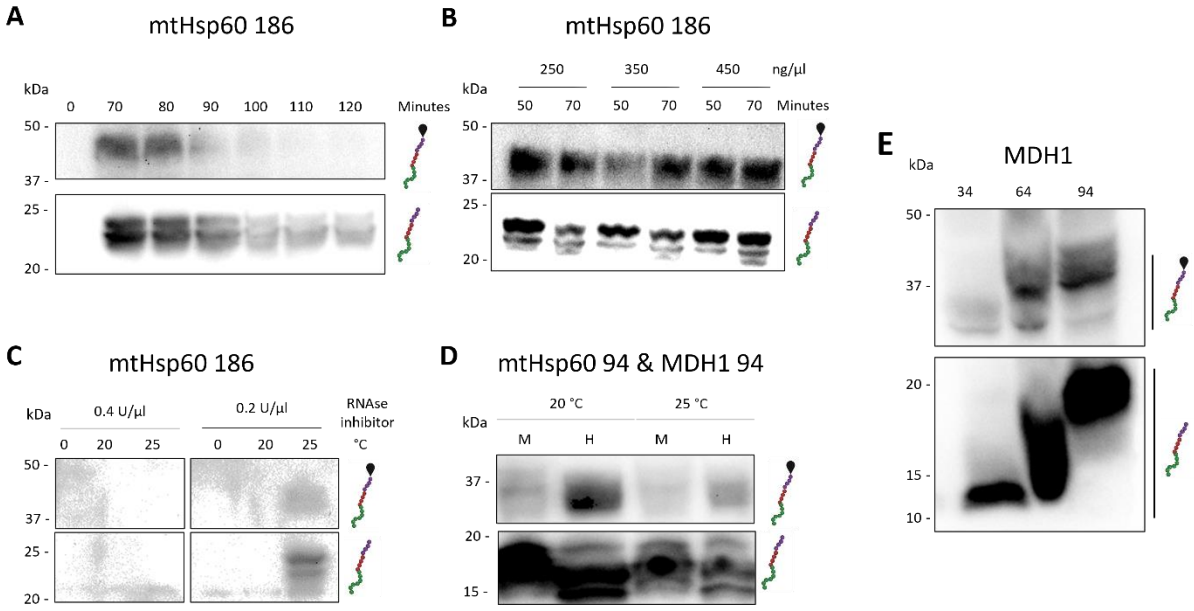

Figure 7 Optimization of the yeast lysate *in vitro* translation system anti-FLAG western blot of *in vitro* translation reactions using mtHsp60 168 showing **A)** time intervals, **B)** time intervals and mRNA concentrations, **C)** RNAse inhibitor concentrations. **D)** anti-FLAG western blot of two different temperatures in an *in vitro* translation reaction using mtHsp60 94 and MDH1 94 (M: MDH1, H: mtHsp60). **E)** anti-FLAG western blot of MDH1 truncation in *in vitro* translation reactions under optimized conditions. (Upper cartoon signifies peptidyl-tRNA nascent chain and lower cartoon signifies free nascent chain).

3.3.2 Ribosome isolation and RNC affinity purification from yeast lysate

To isolate the ribosomes and purify the yeast-derived RNCs, the protocol from RRL (**Figure 5A**) was applied to yeast *in vitro* translation reactions. 200 µl of MDH1 34 *in vitro* translation reaction was loaded onto a 1 M sucrose cushion to separate the RNCs/ribosomes from the free nascent chains. (**Figure 8A**). The ribosomes are efficiently isolated from the translation mix since the pellet fraction does not contain any nascent chain signal (**Figure 8A lane 3**). In contrast, the supernatant does (**Figure 8A lane 2**). Negative stain EM of the pellet fraction was performed to validate if 80s ribosomes are present in the sample (**Figure 8B**). At a concentration of 70 nM, the ribosome sample is homogenously distributed without any visible aggregation. The majority of ribosomes also appear as 80S ribosomes, and for some, the 40s and 60s subunit can be observed (**Figure 8C**).

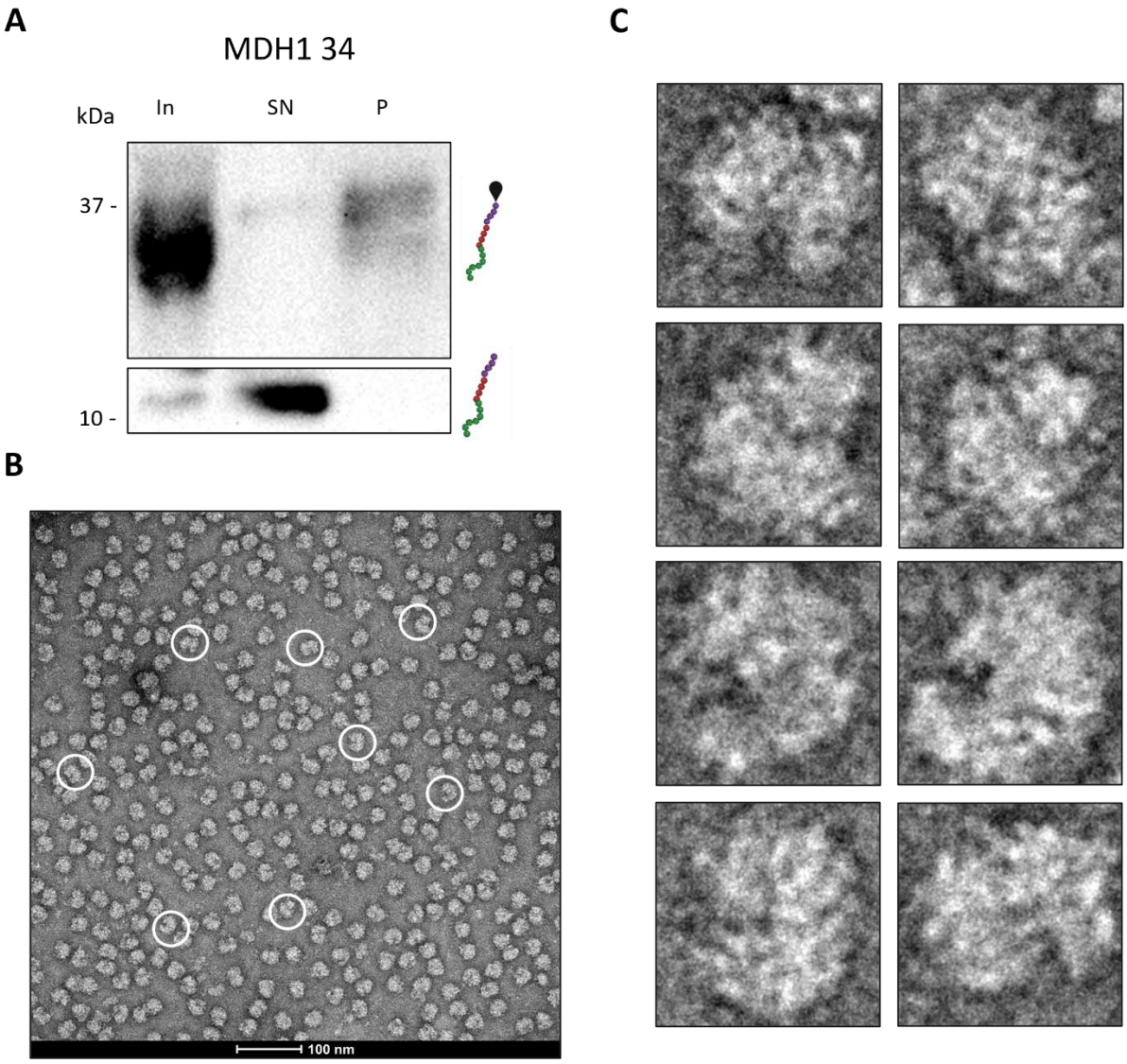

Figure 8. Ribosome isolation and affinity purification of RNCs containing MDH1 34 A) anti-FLAG western blot imaging of MDH1 32 after *in vitro* translation and ultracentrifugation. (In: Input, SN: Supernatant, P: Pellet) **B)** Negative stain EM image at 73 000 x magnification of the MDH1 32 RNC/ribosome sample at 70 nM concentration. White circles indicate ribosomes with visible 40s and 60s subunits, which are displayed in **(C).** (Upper cartoon signifies peptidyl-tRNA nascent chain and lower cartoon signifies free nascent chain).

The affinity purification protocol was adapted from section 3.2.2 to be applied to yeast lysate. 200 µl of *in vitro* translation reaction was ultracentrifuged, the RNC/ribosome pellet was resolubilized in 300 µl bead compatible buffer, and pulled down using 50 µl beads (**Figure 9A**). There is still a signal left in the flowthrough fraction (**Figure 9A, lane 2**), suggesting that the number of beads is insufficient for the number of RNCs in the resolubilized RNC/ribosome pellet. Similar to the RRL-derived RNCs, there is no signal in the elution fraction (**Figure 9A lane 5**). However, there is signal in the beads fraction (**Figure 9A lane 6**), again suggesting that the RNCs bind unspecifically and not through the S1 aptamer. This was complemented by data from the construct lacking the S1 aptamer (**Figure 9B lane 5 and 6**). Surprisingly, the peptidyl t-RNA signal for the construct lacking the S1 aptamer runs lower (**Figure 9B lane 6**) than the one containing the aptamer (**Figure 9A lane 6**), even though the protein is the same.

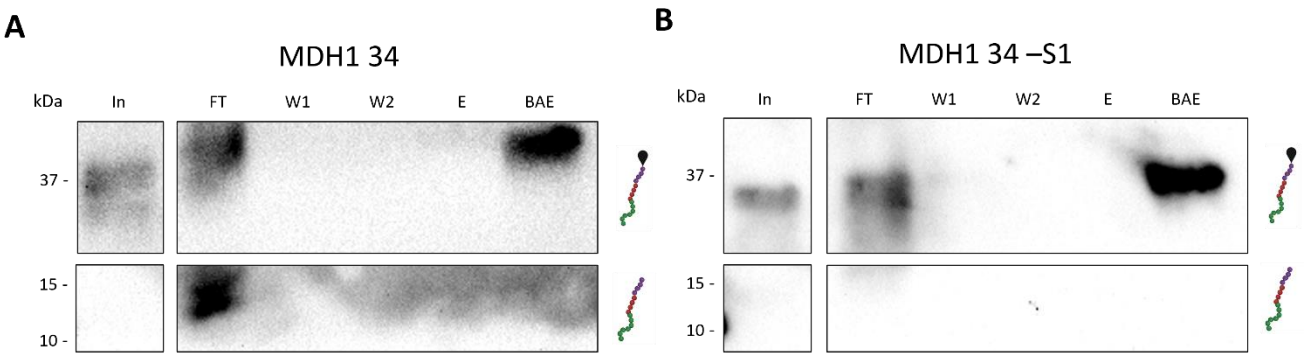

Figure 9. Affinity purification of MDH1 34 RNCs A) Anti-FLAG western blot of RNC pulldown of MDH1 34 ribosome pellet sample via the S1 aptamer **B)** Anti-FLAG western blot of RNC pulldown of MDH1 34 ribosome pellet sample lacking the S1 aptamer (In: Input, FT: Flowthrough, W1: Wash 1, W2: Wash 2, E: Elution, BAE: Beads after elution). (Upper cartoon signifies peptidyl-tRNA nascent chain and lower cartoon signifies free nascent chain).

4 Discussion and outlook

4.1 Generation of a purified RRL RNC sample

To identify potential co-translational targeting factors in mammals *in vitro*, we generated stalled RNC complexes translating truncations of the mitochondrial preprotein OTC (**Figure 4A**). The truncations were expressed efficiently in an in-house transcription and translation system, except for the smallest OTC 20 truncation (**Figure 4A lane 7**). To image the OTC truncations, autoradiography was used. A requirement for signal using this method is the inclusion of [^{35}S] labeled methionine and cysteine in the translated protein. Looking at the first 20 amino acids of OTC (MLFNLRILLNNAAFRNGHNF), there is only one methionine in the primary sequence and no cysteine. Therefore, another possible scenario could be that the OTC 20 truncation was expressed in RRL, however not visible in autoradiography.

The inclusion of this particular truncation was based on cross-linking evidence of NAC already interacting with the nascent chain inside the ribosomal exit tunnel at a length of 20 amino acids (Gamerdinger et al., 2019). Therefore, the OTC 20 truncation needs to remain at this length, and the addition of a FLAG tag for Western blot imaging is consequently unfavorable. The OTC 20 template could be adapted by replacing the last three amino acids with methionine or cysteine to improve the potential signal. This number of replacements should be enough to provide a signal since the OTC 32 construct (**Table S1, construct 89**) contains three methionines and one cysteine and shows a clear signal in the autoradiography images (**Figure 4A lane 6**). An additional scenario could be that the mRNA of the OTC 20 construct is too small to be stable, which is indicated by several faint bands (**Figure 4A lane 7**).

Isolated ribosome samples from OTC 32 and OTC 82 *in vitro* translation reactions were visually inspected using negative stain EM (**Figure 4 C&D**). Both samples were not homogeneously distributed on the grid, and the OTC 82 RNC sample showed clusters of ribosomes, most likely formed due to aggregation or insufficient resuspension after ultracentrifugation. One reason for the high amount of aggregation in the OTC 82 sample compared to the OTC 32 sample could have been the staining. For the OTC 32 sample, the uranyl acetate had been spun down; this was not the case for the OTC 82 sample. Another reason could be that there were fewer ribosomes in the OTC 32 sample, as indicated by the low signal in the western blot (**Figure 4B lane 1**) compared to the signal for the OTC 82 sample (**Figure 4B lane 2**).

On the Cu 300 Quantifoil R 2/2 grids with an additional 4 nm carbon film, the OTC 32 sample was also aggregating (**Figure S2 B&C**). Moreover, the OTC 32 sample was not homogeneously distributed on the grid. After this observation, the buffer used to resuspend the pellet after ultracentrifugation was adapted to include 50 mM NaCl and 1mM DTT, which was previously absent in the buffer. In addition, additional resuspension steps were added. Samples generated in this way were imaged on Quantifoil Holey R 2/1 Cu 200 grids under cryogenic conditions (**figure S2D**). The sample was slightly more homogenously distributed on the ice; however, still far from optimal. For the imaging of the *C.elegans* 60s ribosomes performed by (Gamerdinger et al., 2019), the same grid type was used, but they allowed for a 40 second incubation time of the sample on the grid before blotting it off. Applying and optimizing this incubation time could improve the distribution of the OTC 32 RNCs on the grid. Once the grid conditions are optimized, cryo-SPA-EM can determine the ratio between empty ribosomes and RNCs after 15 minutes of translation. Moreover, if a significant proportion of RNCs, compared to empty ribosomes, is present in the sample, initial data processing could provide insights into the presence of potential densities corresponding to potential targeting factors.

To enrich for the desired RNCs, affinity purification was attempted on the RNC OTC 32 sample through an S1 RNA aptamer incorporated into the 3' UTR (**Figure 5 B&C**). The purification protocol attempted in this work has thus far not resulted in purified and enriched RNC samples. There was no signal present in the beads before the elution and elution fractions. Looking at the ribosome input for this particular affinity purification (**Figure 5B lane 1**), the signal for the stalled ribosomes is very low, especially compared to **figure S2A**. This could explain why the signal in the other lanes is also low or not even visible. One reason for this could have been issues with the RRL translation mixture following preparation by different users, which had occurred before.

The experiment also showed that the RNCs bind unspecifically to the beads (**Figure 5B & C lane 7**) as they could not be released by elution with 5 mM biotin. It is unknown to what amount unspecific binding occurred, so the biotin elution concentration should be increased. To prevent unspecific binding in future experiments, salt concentrations in the washing buffer should be increased from 150 mM to 250-300 mM, which has been used before in purifications using the S1 aptamer (Dong et al., 2015). However, the S1 aptamer has not been used in the context of RNCs before, and therefore other salt conditions in the binding buffer and elution buffer should also be explored. In addition, sepharose beads instead of magnetic beads could be used. In previous work performed by L.M.K. Thärichen (Sinning Lab, BZH Heidelberg University) RNC purification was performed using nickel Sepharose beads. In this experiment, the RNCs did not stick to the beads, suggesting that the stickiness might come from the magnetic beads.

However, since this experiment does not show that the RNCs bind through a specific interaction, it should also be considered that the S1 tag might not be accessible for the streptavidin beads. The placement of the S1 aptamer was based on secondary structure predictions for the 3'UTR to prevent S1 aptamer localization in a folded RNA section. This could be an inadequate prediction. The binding of the S1 aptamer to the streptavidin beads could be improved by putting an additional S1 aptamer in the 3'UTR. Another option would be to put an N-terminal protein encoded tag on the nascent chain. One significant objection to this addition would be that early interactions between NAC/other targeting factors and the MTS could be affected.

Additionally, an option could be to omit the affinity purification completely. With cryo-SPA-EM analysis of the RNCs/ribosome sample after ultracentrifugation, we might also obtain enough signal to see the nascent chain in the ribosomal exit tunnel and targeting factors. This is, however, dependent on the ratio between RNCs and ribosomes. This ratio could be estimated by Western blot using an antibody against a ribosomal protein. The signal for this ribosomal protein can then be compared to the RNC signal, thus estimating the number of RNCs. If a significant amount of RNCs is present in the sample, affinity purification could be omitted.

4.2 Generation of a purified RNA sample from yeast lysate

Before RNCs could be generated in a yeast lysate *in vitro* translation system, the system itself was established and optimized from the wildtype *S.cerevisiae* S288C yeast strain (**Figure 6**). For the optimization, truncated versions of MDH1 and mtHsp60 were used. Interestingly, as shown in **Figure 6D**, MDH1 was expressed in a lower amount than mtHsp60, which could be explained by a difference in mRNA 5'UTR secondary structure. This secondary structure difference can result in a different translation initiation rate and thus a different amount of protein output (Mauger et al., 2019). Additionally, the buffer component requirements could differ for each mRNA. Still, MDH1 was chosen to optimize the protocol further since there is more substantial evidence that MDH1 import into the mitochondria depends on NAC and co-translationally imported into the mitochondria (Fünfschilling & Rospert, 1999; Lesnik et al., 2014). For mtHsp60, cross-linking data has only shown that NAC interacts with the MTS of mtHsp60 in RRL (Gamerdinger et al., 2019). During the optimization process, multiple

bands for the nascent chain were visible in all the experiments. Furthermore, two bands were visible for the peptidyl-tRNA signal in MDH1 34, 64, and 94 (**Figure 7E**). These additional bands for the nascent chain were also observed in earlier work using this system performed by L.M.K. Thärichen (Sinning Lab, BZH Heidelberg University). During the cryo-milling step of the yeast lysate preparation, organelle membranes are also destroyed. Therefore, MPP is free in the lysate and could be active during the translation reaction. The size difference between these nascent chain bands could correspond to the size of the MTS, and the different bands might therefore correspond to the preprotein and the mature protein after cleavage with MPP. Since RNCs are separated from the other free nascent chains during the ultracentrifugation step, these additional bands are not deemed problematic. The additional bands for the peptidyl t-RNA are not removed during the ultracentrifugation step. However, they are only observed in **Figure 7E** before ultracentrifugation and no longer after (**Figure 8A lane 3**).

The MDH1 34 RNCs ribosomes population was isolated from the yeast translation mixture in the same way as the RRL-derived RNCs (**Figure 8A lane 3**). The MDH1 34 sample was also inspected using negative stain-EM in the RNC buffer described in section 2.9 (**Figure 8 B&C**). Using this buffer, the ribosomes are homogeneously distributed on the grid and appeared as stable 80s ribosomes. Additionally, affinity purification of the yeast-derived RNCs was also attempted, similar to the strategy for RRL-derived RNCs (**Figure 9**). The result of this pulldown is similar as for the RRL-derived RNCs since the yeast-derived RNCs were also unspecifically bound to the streptavidin beads (**Figure 9 A&B lane 6**). The same optimizations for the RRL-derived RNC purification can be applied for the yeast-derived RNCs.

4.3 Outlook

In this thesis, a yeast *in vitro* translation system was established and optimized. In addition, truncated RNCs for both mammalian and yeast model proteins were successfully generated in RRL and yeast *in vitro* translation systems, respectfully. RNCs generated with model proteins OTC and MDH1 were visually inspected using negative stain EM. Moreover, affinity purification was attempted to obtain an enriched RNC sample.

Optimizations still need to be done before both the RRL and yeast-derived RNCs can be used to study early co-translational targeting. Firstly, the RNC buffer needs to be optimized for RNC stability and solubility. Additionally, the affinity pulldown protocol needs to be optimized for RRL and yeast-derived RNCs. As previously shown using the RRL-derived RNCs, grid conditions for imaging under cryogenic conditions remain far from optimal and also need to be optimized for RRL and yeast-derived RNCs.

When all the conditions are optimized, cryo-SPA-EM would be the next step to obtain structural data on co-translational targeting factors in mammals and yeast in the context of co-translational mitochondrial import. Cross-linking mass spectrometry would be needed for density identification to determine which factors interact with the RNCs. After this determination, factors of which protein models exist can be modeled into the EM density if they are well resolved in the reconstructions.

In addition to investigating early co-translational targeting factors, the RNC generation and purification protocol could be used to study those RNCs in the context of co-translational protein import on the mitochondrial membrane.

Lastly, the establishment of the yeast *in vitro* translation system in the lab allows for the application of this system in other research fields, such as *S,cerevisiae* protein import into the ER.

5 Supplementary

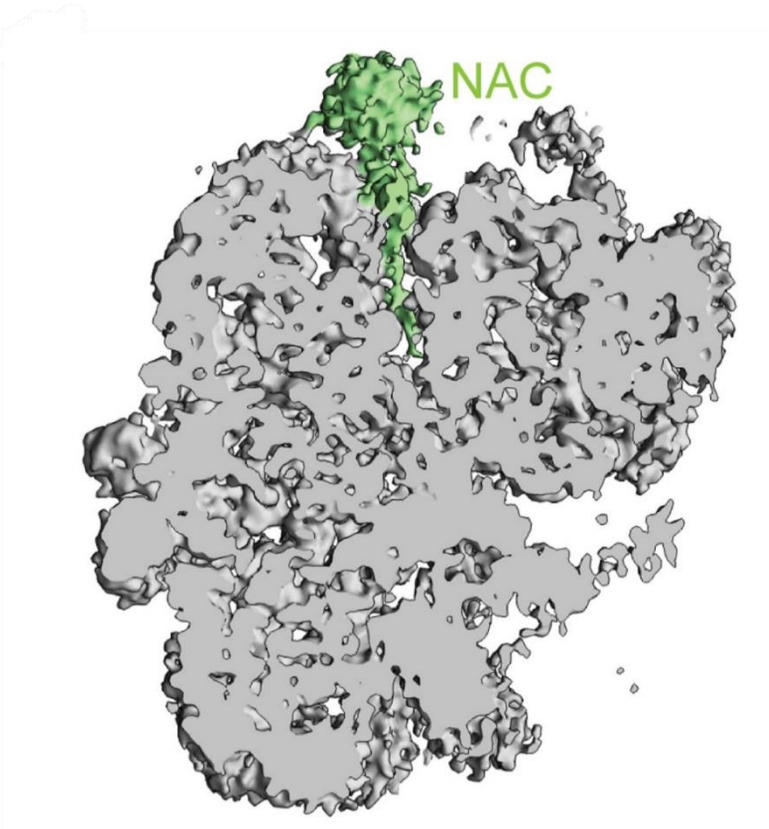

Figure S1 Electron density of the 60S *C.elegans* Ribosome-NAC complex. A subunit of NAC inserts itself into the ribosomal exit tunnel to probe for nascent chains. Figure adapted from (Gamerdinger et al., 2019)

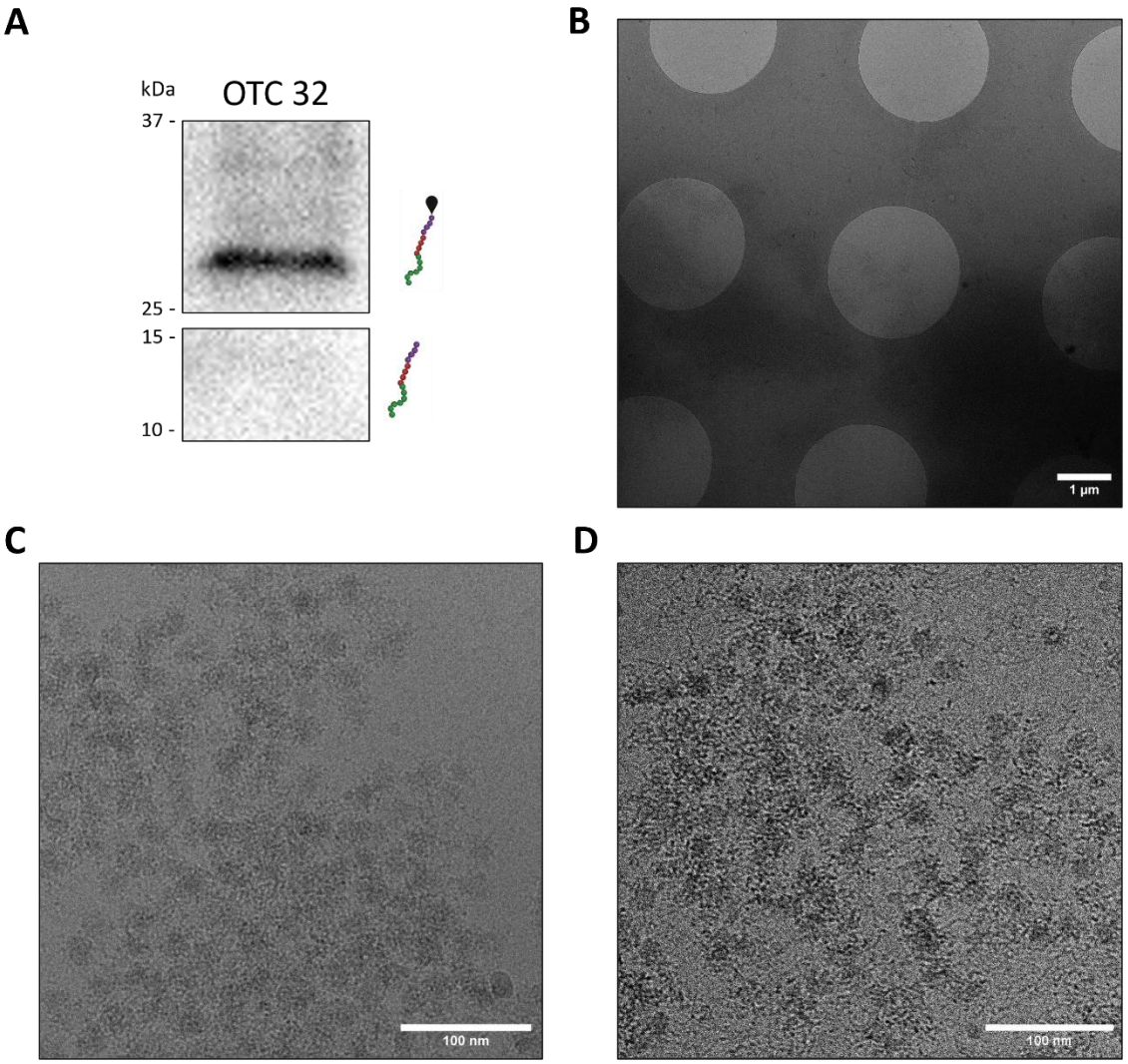

Figure S2. Cryo EM of the OTC 32 RNC/ribosome sample A) anti-FLAG western blot of OTC 32 ribosome pellets after *in vitro* translation and ribosome isolation. **B)** 5600 x magnification micrograph of OTC 32 RNC/ribosome pellets at OD260 of 2 mAU. **C)** 130 000 x magnification micrograph of OTC 32 ribosome pellets at OD260 of 2 mAU **D)** 130 000 x magnification micrograph of OTC 32 ribosome pellets at OD260 of 4 mAU

Table S1: Information on plasmids and constructs used and generated

ID	NAME	Plasmid	Antibiotic resistance	Protein sequence
52	Yeast Hsp60(1-186)-HA-CMV	pMA-t	Amp	MLSRVAKRAFSSTVANPYKVTVLGAGGGIGQPLSLLLKLNHKVTDLRLYDLKGAKGVATDLSHIPTNSVVKGFTPEEPDGLNNALKDTDMVLIPAGVPRKPGMTRDDLFAINASIVRDLAAATAESAPNAAILVISNPVNSTVPIVAQVLKNKGVYNPKKLFGVTTLDSIRAARFISEVENTDPTQYPYDVPDYAMEPLVLSAKKLSSLLTCKYIPP*
53	Yeast MDH1(1-186)-HA-CMV	pMX-RQ	Kan	MLRSSVVRSRATLRPLLRRAYSSHKELKFGVEGRASLLKGVETLAEAVAATLGPKGRNVLIEQPFGPPKITKDGVTVAKSIVLKDKFENMGAKLLQEVASKTNEAAGDGTTSATVLGRAIFTESVKNVAAGCNPMDLRRGSQVAVEKVIEFLSANKKEITTSEEIAQVATISANGDSHVGKLLASAYPYDVPDYAMEPLVLSAKKLSSLLTCKYIPP*
70	pOTC(1-92)-2xFLAG-CMV-S1strep	pMX	Amp	MLFNLRILLNNAAFRNGHNFMVRNFRCGQPLQNKVQLKGRDLLTLKNFTGEEIKYMLWLSADLKFRIKQKGEYLPLLQGKSLGMIFEKRSTRDYKDDDDKDYKDDDDKMEPLVLSAKKLSSLLTCKYIPP*
84	pOTC(1-82)-2xFLAG-CMV S1strep	pMX	Amp	MLFNLRILLNNAAFRNGHNFMVRNFRCGQPLQNKVQLKGRDLLTLKNFTGEEIKYMLWLSADLKFRIKQKGEYLPLLQGKSLDYKDDDDKDYKDDDDKMEPLVLSAKKLSSLLTCKYIPP*
85	pOTC(1-72)-2xFLAG-CMV-S1strep	pMX	Amp	MLFNLRILLNNAAFRNGHNFMVRNFRCGQPLQNKVQLKGRDLLTLKNFTGEEIKYMLWLSADLKFRIKQKGEDYKDDDDKDYKDDDDKMEPLVLSAKKLSSLLTCKYIPP*
86	pOTC(1-62)-2xFLAG-CMV-S1strep	pMX	Amp	MLFNLRILLNNAAFRNGHNFMVRNFRCGQPLQNKVQLKGRDLLTLKNFTGEEIKYMLWLSADDYKDDDDKDYKDDDDKMEPLVLSAKKLSSLLTCKYIPP*
87	pOTC(1-52)-2xFLAG-CMV-S1strep	pMX	Amp	MLFNLRILLNNAAFRNGHNFMVRNFRCGQPLQNKVQLKGRDLLTLKNFTGEEDYKDDDDKDYKDDDDKMEPLVLSAKKLSSLLTCKYIPP*
88	pOTC(1-42)-2xFLAG-CMV-S1strep	pMX	Amp	MLFNLRILLNNAAFRNGHNFMVRNFRCGQPLQNKVQLKGRDLDYKDDDDKDYKDDDDKMEPLVLSAKKLSSLLTCKYIPP*
89	pOTC(1-32)-2xFLAG-CMV-S1strep	pMX	Amp	MLFNLRILLNNAAFRNGHNFMVRNFRCGQPLQDYKDDDDKDYKDDDDKMEPLVLSAKKLSSLLTCKYIPP*

ID	NAME	Plasmid	Antibiotic resistance	Protein sequence
90	Yeast MDH1(1-186)-2xFLAG-CMV	pMX-RQ	Kan	MLSRVAKRAFSSTVANPYKVTVLGAGGGIGQPLSLLLKLNHKVTDLRLYDLKGAKGVATDLSHIPTNSVVKGFTPEEPDGLNNALKDTDMVLIPAGVPRKPGMTRDDLFAINASIVRDLAAATAESAPNAAILVISNPVNSTVPIVAQVLKNKGVYNPKKLFGVTTLDSIRAARFISEVENTDPTQDYKDDDDKDYKDDDDKMEPLVLSAKKLSSLLTCKYIPP*
91	Yeast Hsp60(1-186)-2xFLAG-CMV	pMA-t	Amp	MLRSSVVRSRATLRPLLRRAYSSHKELKFGVEGRASLLKGVETLAEAVAATLGPKGRNVLIEQPFGPPKITKDGVTVAKSIVLKDKFENMGAKLLQEVASKTNEAAGDGTTSATVLGRAIFTESVKNVAAGCNPMDLRRGSQVAVEKVIEFLSANKKEITTSEEIAQVATISANGDSHVGKLLASADYKDDDDKDYKDDDDKMEPLVLSAKKLSSLLTCKYIPP*
96	Yeast MDH1(1-186)-2xFLAG-CMV-S1strep	pMX-RQ	Kan	MLSRVAKRAFSSTVANPYKVTVLGAGGGIGQPLSLLLKLNHKVTDLRLYDLKGAKGVATDLSHIPTNSVVKGFTPEEPDGLNNALKDTDMVLIPAGVPRKPGMTRDDLFAINASIVRDLAAATAESAPNAAILVISNPVNSTVPIVAQVLKNKGVYNPKKLFGVTTLDSIRAARFISEVENTDPTQDYKDDDDKDYKDDDDKMEPLVLSAKKLSSLLTCKYIPP*
97	Yeast Hsp60(1-186)-2xFLAG-CMV-S1strep	pMA-t	Amp	MLRSSVVRSRATLRPLLRRAYSSHKELKFGVEGRASLLKGVETLAEAVAATLGPKGRNVLIEQPFGPPKITKDGVTVAKSIVLKDKFENMGAKLLQEVASKTNEAAGDGTTSATVLGRAIFTESVKNVAAGCNPMDLRRGSQVAVEKVIEFLSANKKEITTSEEIAQVATISANGDSHVGKLLASADYKDDDDKDYKDDDDKMEPLVLSAKKLSSLLTCKYIPP*
112	Yeast 5'UTR-MDH1 (1-186)-2xFLAG-CMV-S1strep	pMX-RQ	Kan	MLSRVAKRAFSSTVANPYKVTVLGAGGGIGQPLSLLLKLNHKVTDLRLYDLKGAKGVATDLSHIPTNSVVKGFTPEEPDGLNNALKDTDMVLIPAGVPRKPGMTRDDLFAINASIVRDLAAATAESAPNAAILVISNPVNSTVPIVAQVLKNKGVYNPKKLFGVTTLDSIRAARFISEVENTDPTQDYKDDDDKDYKDDDDKMEPLVLSAKKLSSLLTCKYIPP*
113	Yeast 5'UTR-Hsp60(1-186)-2xFLAG-CMV-S1strep	pMA-t	Amp	MLRSSVVRSRATLRPLLRRAYSSHKELKFGVEGRASLLKGVETLAEAVAATLGPKGRNVLIEQPFGPPKITKDGVTVAKSIVLKDKFENMGAKLLQEVASKTNEAAGDGTTSATVLGRAIFTESVKNVAAGCNPMDLRRGSQVAVEKVIEFLSANKKEITTSEEIAQVATISANGDSHVGKLLASADYKDDDDKDYKDDDDKMEPLVLSAKKLSSLLTCKYIPP*
117	Yeast 5'UTR-MDH1 (1-94)-2xFLAG-CMV-S1strep	pMX-RQ	Kan	MLSRVAKRAFSSTVANPYKVTVLGAGGGIGQPLSLLLKLNHKVTDLRLYDLKGAKGVATDLSHIPTNSVVKGFTPEEPDGLNNALKDTDMVLIPDYKDDDDKDYKDDDDKMEPLVLSAKKLSSLLTCKYIPP*

ID	NAME	Plasmid	Antibiotic resistance	Protein sequence
118	Yeast 5'UTR-MDH1 (1-84)-2xFLAG-CMV-S1strep	pMX-RQ	Kan	MLSRVAKRAFSSTVANPYKVTVLGAGGGIGQPLSLLLKLNHKVTDLRLYDLKGAKGVATDLSHIPTNSVVKGFTPEEPDGLNNADYKDDDDKDYKDDDDKMEPLVLSAKKLSSLLTCKYIPP*
119	Yeast 5'UTR-MDH1 (1-74)-2xFLAG-CMV-S1strep	pMX-RQ	Kan	MLSRVAKRAFSSTVANPYKVTVLGAGGGIGQPLSLLLKLNHKVTDLRLYDLKGAKGVATDLSHIPTNSVVKGFTDYKDDDDKDYKDDDDKMEPLVLSAKKLSSLLTCKYIPP*
120	Yeast 5'UTR-MDH1 (1-64)-2xFLAG-CMV-S1strep	pMX-RQ	Kan	MLSRVAKRAFSSTVANPYKVTVLGAGGGIGQPLSLLLKLNHKVTDLRLYDLKGAKGVATDLSHIDYKDDDDKDYKDDDDKMEPLVLSAKKLSSLLTCKYIPP*
121	Yeast 5'UTR-MDH1 (1-54)-2xFLAG-CMV-S1strep	pMX-RQ	Kan	MLSRVAKRAFSSTVANPYKVTVLGAGGGIGQPLSLLLKLNHKVTDLRLYDLKGADYKDDDDKDYKDDDDKMEPLVLSAKKLSSLLTCKYIPP*
122	Yeast 5'UTR-MDH1 (1-44)-2xFLAG-CMV-S1strep	pMX-RQ	Kan	MLSRVAKRAFSSTVANPYKVTVLGAGGGIGQPLSLLLKLNHKVTDYKDDDDKDYKDDDDKMEPLVLSAKKLSSLLTCKYIPP*
123	Yeast 5'UTR-MDH1(1-34)-2xFLAG-CMV-S1strep	pMX-RQ	Kan	MLSRVAKRAFSSTVANPYKVTVLGAGGGIGQPLSDYKDDDDKDYKDDDDKMEPLVLSAKKLSSLLTCKYIPP*
124	Yeast 5'UTR-Hsp60(1-94)-2xFLAG-CMV-S1strep	pMA-t	Amp	MLRSSVVRSRATLRPLLRRAYSSHKELKFGVEGRASLLKGVETLAEAVAATLGPKGRNVLIEQPFGPPKITKDGVTVAKSIVLKDKFENMGAKLDYKDDDDKDYKDDDDKMEPLVLSAKKLSSLLTCKYIPP*
125	Yeast 5'UTR-Hsp60(1-84)-2xFLAG-CMV-S1strep	pMA-t	Amp	MLRSSVVRSRATLRPLLRRAYSSHKELKFGVEGRASLLKGVETLAEAVAATLGPKGRNVLIEQPFGPPKITKDGVTVAKSIVLKDYKDDDDKDYKDDDDKMEPLVLSAKKLSSLLTCKYIPP*
126	Yeast 5'UTR-Hsp60(1-74)-2xFLAG-CMV-S1strep	pMA-t	Amp	MLRSSVVRSRATLRPLLRRAYSSHKELKFGVEGRASLLKGVETLAEAVAATLGPKGRNVLIEQPFGPPKITKDGDYKDDDDKDYKDDDDKMEPLVLSAKKLSSLLTCKYIPP*
127	Yeast 5'UTR-Hsp60 (1-64)-2xFLAG-CMV-	pMA-t	Amp	MLRSSVVRSRATLRPLLRRAYSSHKELKFGVEGRASLLKGVETLAEAVAATLGPKGRNVLIEQPDYKDDDDKDYKDDDDKMEPLVLSAKKLSSLLTCKYIPP*

S1strep

ID	NAME	Plasmid	Antibiotic resistance	Protein sequence
128	Yeast 5'UTR-Hsp60(1-54)-2xFLAG-CMV-S1strep	pMA-t	Amp	MLRSSVVRSRATLRPLLRRAYSSHKELKFGVEGRASLLKGVETLAEAVAATLGPDYKDDDDKDYKDDDDKMEPLVLSAKKLSSLLTCKYIPP*
129	Yeast 5'UTR-Hsp60(1-44)-2xFLAG-CMV-S1strep	pMA-t	Amp	MLRSSVVRSRATLRPLLRRAYSSHKELKFGVEGRASLLKGVETLDYKDDDDKDYKDDDDKMEPLVLSAKKLSSLLTCKYIPP*
130	Yeast 5'UTR-Hsp60(1-34)-2xFLAG-CMV-S1strep	pMA-t	Amp	MLRSSVVRSRATLRPLLRRAYSSHKELKFGVEGRDYKDDDDKDYKDDDDKMEPLVLSAKKLSSLLTCKYIPP*

Tabel S2: primer sequences used

ID	Primer name	Sequence (5'-3')
LMKT32	pOTCrevlong	ATGAGGCCAGTCTTGTGCTCCGAGCTCG
LMKT40	pOTCfwd	CGAATTGGCGGAAGGCCGTCAAGG
LMKT165	2xFLAG fwd	GACTACAAGGACGACGATGACAAGGACTACAAGG
LMKT166	humanpOTC rev 1-82	TAAGGACTTCCCTTGCAATAAAGGCAAATACTCTCC
LMKT167	humanpOTC rev 1-72	CTCTCCTTTCTGTTTTATCCTAAATTTCAGATCTGCTGATAGCC
LMKT168	humanpOTC rev 1-62	ATCTGCTGATAGCCATAGCATATATTTAATTTCTTCTCCGG
LMKT169	humanpOTC rev 1-52	TTCTTCTCCGGTAAAGTTTTTTAGAGTGAGAAGGTCACGGC
LMKT170	humanpOTC rev 1-42	AAGGTCACGGCCCTTCAGCTGCAC
LMKT171	humanpOTC rev 1-32	TTGTAGTGGTTGTCCACACCGAAAATTTCGAACC
LMKT178	FLAG tag insert fwd	GACTACAAGGACGACGATGACAAGATGGAACCGCTGGTGCTGAG
LMKT179	FLAG tag insert MDH1 rev	CTTGTCATCGTCGTCCTTGTAGTCCTGAGTTGGATCGGTGTTCTCGACTTCTG
LMKT180	FLAG tag insert Hsp60 rev	CTTGTCATCGTCGTCCTTGTAGTCAGCTGAAGCTAGTAACTTACCAACATGAGAG
LMKT183	S1 insert MDH1 fwd	ACCGACCAGAATCATGCAAGTGCGTAAGATAGTCGCGGGCCGGGACTAGAGAAAAATTCATGCTATTCGTTGC
LMKT184	S1 insert MDH1 rev	TGATTTTTGGCAGTTTCCTTCCTTTC
LMKT185	S1 insert Hsp60 fwd	TCTTTCGTTTAAATATGGTAATAATTTTATTATCTTG
LMKT186	S1 insert Hsp60 rev	CCCGGCCCGCGACTATCTTACGCACTTGCATGATTCTGGTCGGTTAAATTTTGAATTAAGGCGGTCG
LMKT191	YeastpMDH1 rev 1-94	AGGAATTAAAACCATGTCTGTGTCCTTTAAAGCGTTGTTC
LMKT192	YeastpMDH1 rev 1-84	AGCGTTGTTCAATCCGTCTGGCTCTTC
LMKT193	YeastpMDH1 rev 1-74	AGTAAACCCCTTGACCACGGAGTTTGTTGG
LMKT194	YeastpMDH1 rev 1-64	AATATGAGACAAATCGGTGGCAACACCTTTTGCGCCC
LMKT195	YeastpMDH1 rev 1-54	TGCGCCCTTTAGGTCGTACAGTCTTAAGTCCG
LMKT196	YeastpMDH1 rev 1-44	CGTGACTTTATGGTTAAGCTTTAGAAGCAAAGACAATGGTTGTCC
LMKT197	YeastpMDH1 rev 1-34	AGACAATGGTTGTCCAATACCACCGCCTGC
LMKT198	YeastpHsp60 rev 1-94	TAACTTGGCACCCATATTTTCAAACTTGTCCTTCAACACAATAG
LMKT199	YeastpHsp60 rev 1-84	CTTCAACACAATAGATTTGGCAACTGTAACACCATCC
LMKT200	YeastpHsp60 rev 1-74	ACCATCCTTAGTAATCTTTGGAGGACCGAAAGGC

ID	Primer name	Sequence (5’-3’)
LMKT201	YeastpHsp60 rev 1-64	AGGCTGTTCGATTAAAACGTTTCTACCCTTTGGACCC
LMKT202	YeastpHsp60 rev 1-54	TGGACCCAAAGTAGCAGCAACCGCTTC
LMKT203	YeastpHsp60 rev 1-44	TAAAGTTTCGACACCCTTAAGAAGGGAGGCTCTTCC
LMKT204	YeastpHsp60 rev 1-34	TCTTCCTTCTACACCGAATTTCAATTCTTTATGAGAGGAGTAAGCACG
LMKT205	Excluding S1 in OTC 3’UTR	TTTAGGTAATAAGCATAGATTACACTTAATGGCTTAGACATTATAC
LMKT215	YeastpMDH1 amp fwd	TAAGTTGGGTAACGCCAGGGTTTTCCCAGGCGAATTGAAGGAAGGCCGTC
LMKT216	YeastpHsp60 amp fwd	AAGTTGGGTAACGCCAGGGTTTTCCCAGTCCGTCAAGGCCACGTGTCTTG
LMKT218	YeastpMDH1 5'UTR insert fwd	AGAAAAGGAAGGATACCATATACAATGTTGTCAAGAGTAGCTAAACGTG
LMKT222	Excluding S1 in MDH1 3’UTR	GATGTCGTAATCTCATGATGGCGAGTAG
LMKT231	YeastpMDH1 amp rev	CTCGTAAACCGAAACGTTTATTCATCATTATC
LMKT233	YeastpHsp60 amp rev	GCTCCAGGTACCGAATTCACATTGTATTTACAAG
LMKT260	YeastpMDH1 5’UTR insert rev	TTTGTTTTTTTTCTTCCTTTCCGTACCCTATAGTGAGTCGTATTAATGCG
LMKT261	YeastpHsp60 4’UTR insert fwd	ACATCATAAGCAAAAAAGTTTTCAAAATGTTGAGATCATCCGTTGTTCG
LMKT262	YeastpHsp60 4’UTR insert fwd	TTTCTCGTGGGAATTTTCTTATATCCCTATAGTGAGTCGTATTAGAGCTC
LMKT265	Human pOTC 20 aa rev	GAATTGGCGGAAGGCCGTC
LMKT266	Human pOTC 20 aa fwd	GAAGTTGTGACCATTTCTAAAAGCTGC

6 References

Abe, Y., Shodai, T., Muto, T., Mihara, K., Torii, H., Nishikawa, S., Endo, T., & Kohda, D. (2000). Structural Basis of Presequence Recognition by the Mitochondrial Protein Import Receptor Tom20. *Cell*, *100*(5), 551–560. https://doi.org/10.1016/S0092-8674(00)80691-1

Alamo, M. del, Hogan, D. J., Pechmann, S., Albanese, V., Brown, P. O., & Frydman, J. (2011). Defining the Specificity of Cotranslationally Acting Chaperones by Systematic Analysis of mRNAs Associated with Ribosome-Nascent Chain Complexes. *PLoS Biology*, *9*(7), e1001100. https://doi.org/10.1371/journal.pbio.1001100

Backes, S., Hess, S., Boos, F., Woellhaf, M. W., Gödel, S., Jung, M., Mühlhaus, T., & Herrmann, J. M. (2018). Tom70 enhances mitochondrial preprotein import efficiency by binding to internal targeting sequences. *Journal of Cell Biology*, *217*(4), 1369–1382. https://doi.org/10.1083/jcb.201708044

Becker, T., Song, J., & Pfanner, N. (2019). Versatility of Preprotein Transfer from the Cytosol to Mitochondria. *Trends in Cell Biology*, *29*(7). https://doi.org/10.1016/j.tcb.2019.03.007

Bhangoo, M. K., Tzankov, S., Fan, A. C. Y., Dejgaard, K., Thomas, D. Y., & Young, J. C. (2007). Multiple 40-kDa Heat-Shock Protein Chaperones Function in Tom70-dependent Mitochondrial Import. *Molecular Biology of the Cell*, *18*(9). https://doi.org/10.1091/mbc.e07-01-0088

Chacinska, A., Koehler, C. M., Milenkovic, D., Lithgow, T., & Pfanner, N. (2009). Importing Mitochondrial Proteins: Machineries and Mechanisms. *Cell*, *138*(4). https://doi.org/10.1016/j.cell.2009.08.005

Dao Duc, K., Batra, S. S., Bhattacharya, N., Cate, J. H. D., & Song, Y. S. (2019). Differences in the path to exit the ribosome across the three domains of life. *Nucleic Acids Research*, *47*(8). https://doi.org/10.1093/nar/gkz106

Deshaies, R. J., Koch, B. D., Werner-Washburne, M., Craig, E. A., & Schekman, R. (1988). A subfamily of stress proteins facilitates translocation of secretory and mitochondrial precursor polypeptides. *Nature*, *332*(6167). https://doi.org/10.1038/332800a0

Dolezal, P. (2006). Evolution of the Molecular Machines for Protein Import into Mitochondria. *Science*, *313*(5785), 314–318. https://doi.org/10.1126/science.1127895

Dong, Y., Yang, J., Ye, W., Wang, Y., Ye, C., Weng, D., Gao, H., Zhang, F., Xu, Z., & Lei, Y. (2015). Isolation of Endogenously Assembled RNA-Protein Complexes Using Affinity Purification Based on Streptavidin Aptamer S1. *International Journal of Molecular Sciences*, *16*(9), 22456–22472. https://doi.org/10.3390/ijms160922456

Earl, C. C., Smith, M. T., Lease, R. A., & Bundy, B. C. (2018). Polyvinylsulfonic acid: A Low-cost RNase inhibitor for enhanced RNA preservation and cell-free protein translation. *Bioengineered*, *9*(1). https://doi.org/10.1080/21655979.2017.1313648

Endo, T., & Yamano, K. (2009). Multiple pathways for mitochondrial protein traffic. *Biological Chemistry*, *390*(8). https://doi.org/10.1515/BC.2009.087

Fox, T. D. (2012). Mitochondrial Protein Synthesis, Import, and Assembly. *Genetics*, *192*(4). https://doi.org/10.1534/genetics.112.141267

Fujiki, M., & Verner, K. (1991). Coupling of protein synthesis and mitochondrial import in a homologous yeast in vitro system. *Journal of Biological Chemistry*, *266*(11). https://doi.org/10.1016/S0021-9258(20)89577-5

Fujiki, M., & Verner, K. (1993). Coupling of cytosolic protein synthesis and mitochondrial protein import in yeast. Evidence for cotranslational import in vivo. *Journal of Biological Chemistry*, *268*(3). https://doi.org/10.1016/S0021-9258(18)53941-7

Fünfschilling, U., & Rospert, S. (1999). Nascent Polypeptide–associated Complex Stimulates Protein Import into Yeast Mitochondria. *Molecular Biology of the Cell*, *10*(10). https://doi.org/10.1091/mbc.10.10.3289

Gamerdinger, M., Hanebuth, M. A., Frickey, T., & Deuerling, E. (2015). The principle of antagonism ensures protein targeting specificity at the endoplasmic reticulum. *Science*, *348*(6231), 201–207. https://doi.org/10.1126/science.aaa5335

Gamerdinger, M., Kobayashi, K., Wallisch, A., Kreft, S. G., Sailer, C., Schlömer, R., Sachs, N., Jomaa, A., Stengel, F., Ban, N., & Deuerling, E. (2019). Early Scanning of Nascent Polypeptides inside the Ribosomal Tunnel by NAC. *Molecular Cell*, *75*(5). https://doi.org/10.1016/j.molcel.2019.06.030

Gao, J., Schatton, D., Martinelli, P., Hansen, H., Pla-Martin, D., Barth, E., Becker, C., Altmueller, J., Frommolt, P., Sardiello, M., & Rugarli, E. I. (2014). CLUH regulates mitochondrial biogenesis by binding mRNAs of nuclear-encoded mitochondrial proteins. *Journal of Cell Biology*, *207*(2), 213–223. https://doi.org/10.1083/jcb.201403129

George, R., Beddoe, T., Landl, K., & Lithgow, T. (1998). The yeast nascent polypeptide-associated complex initiates protein targeting to mitochondria in vivo. *Proceedings of the National Academy of Sciences*, *95*(5). https://doi.org/10.1073/pnas.95.5.2296

George, R., Walsh, P., Beddoe, T., & Lithgow, T. (2002). The nascent polypeptide-associated complex (NAC) promotes interaction of ribosomes with the mitochondrial surface in vivo. *FEBS Letters*, *516*(1–3). https://doi.org/10.1016/S0014-5793(02)02528-0

Gerber, A. P., Herschlag, D., & Brown, P. O. (2004). Extensive Association of Functionally and Cytotopically Related mRNAs with Puf Family RNA-Binding Proteins in Yeast. *PLoS Biology*, *2*(3). https://doi.org/10.1371/journal.pbio.0020079

Hoseini, H., Pandey, S., Jores, T., Schmitt, A., Franz-Wachtel, M., Macek, B., Buchner, J., Dimmer, K. S., & Rapaport, D. (2016). The cytosolic cochaperone Sti1 is relevant for mitochondrial biogenesis and morphology. *The FEBS Journal*, *283*(18). https://doi.org/10.1111/febs.13813

Kellems, R. E., Allison, V. F., & Butow, R. A. (1974). Cytoplasmic type 80 S ribosomes associated with yeast mitochondria. II. Evidence for the association of cytoplasmic ribosomes with the outer mitochondrial membrane in situ. *The Journal of Biological Chemistry*, *249*(10).

Kellems, R. E., Allison, V. F., & Butow, R. A. (1975). Cytoplasmic type 80S ribosomes associated with yeast mitochondria. IV. Attachment of ribosomes to the outer membrane of isolated mitochondria. *Journal of Cell Biology*, *65*(1). https://doi.org/10.1083/jcb.65.1.1

Kellems, R. E., & Butow, R. A. (1972). Cytoplasmic-type 80 S Ribosomes Associated with Yeast Mitochondria. *Journal of Biological Chemistry*, *247*(24). https://doi.org/10.1016/S0021-9258(20)81806-7

Leppek, K., & Stoecklin, G. (2014). An optimized streptavidin-binding RNA aptamer for purification of ribonucleoprotein complexes identifies novel ARE-binding proteins. *Nucleic Acids Research*, *42*(2). https://doi.org/10.1093/nar/gkt956

Lesnik, C., Cohen, Y., Atir-Lande, A., Schuldiner, M., & Arava, Y. (2014). OM14 is a mitochondrial receptor for cytosolic ribosomes that supports co-translational import into mitochondria. *Nature Communications*, *5*(1). https://doi.org/10.1038/ncomms6711

Liu, Y., Hu, Y., Li, X., Niu, L., & Teng, M. (2010). The Crystal Structure of the Human Nascent Polypeptide-Associated Complex Domain Reveals a Nucleic Acid-Binding Region on the NACA Subunit,. *Biochemistry*, *49*(13), 2890–2896. https://doi.org/10.1021/bi902050p

MacKenzie, J. A., & Payne, R. M. (2004). Ribosomes Specifically Bind to Mammalian Mitochondria via Protease-sensitive Proteins on the Outer Membrane. *Journal of Biological Chemistry*, *279*(11). https://doi.org/10.1074/jbc.M307167200

Marc, P., Margeot, A., Devaux, F., Blugeon, C., Corral-Debrinski, M., & Jacq, C. (2002). Genome-wide analysis of mRNAs targeted to yeast mitochondria. *EMBO Reports*, *3*(2). https://doi.org/10.1093/embo-reports/kvf025

Margeot, A., Blugeon, C., Sylvestre, J., Vialette, S., Jacq, C., & Corral-Denrinski, M. (2002). In Saccharomyces cerevisiae, ATP2 mRNA sorting to the vicinity of mitochondria is essential for respiratory function. *The EMBO Journal*, *21*(24). https://doi.org/10.1093/emboj/cdf690

Mauger, D. M., Cabral, B. J., Presnyak, V., Su, S. v., Reid, D. W., Goodman, B., Link, K., Khatwani, N., Reynders, J., Moore, M. J., & McFadyen, I. J. (2019). mRNA structure regulates protein expression through changes in functional half-life. *Proceedings of the National Academy of Sciences*, *116*(48). https://doi.org/10.1073/pnas.1908052116

Mokranjac, D., Sichting, M., Popov-Čeleketić, D., Mapa, K., Gevorkyan-Airapetov, L., Zohary, K., Hell, K., Azem, A., & Neupert, W. (2009). Role of Tim50 in the Transfer of Precursor Proteins from the Outer to the Inner Membrane of Mitochondria. *Molecular Biology of the Cell*, *20*(5). https://doi.org/10.1091/mbc.e08-09-0934

Mukhopadhyay, A., Ni, L., & Weiner, H. (2004). A co-translational model to explain the in vivo import of proteins into HeLa cell mitochondria. *Biochemical Journal*, *382*(1), 385–392. https://doi.org/10.1042/BJ20040065

Murakami, H., Pain, D., & Blobel, G. (1988). 70-kD heat shock-related protein is one of at least two distinct cytosolic factors stimulating protein import into mitochondria. *The Journal of Cell Biology*, *107*(6 Pt 1). https://doi.org/10.1083/jcb.107.6.2051

Neupert, W., & Herrmann, J. M. (2007). Translocation of Proteins into Mitochondria. *Annual Review of Biochemistry*, *76*(1). https://doi.org/10.1146/annurev.biochem.76.052705.163409

Ni, L., Heard, T. S., & Weiner, H. (1999). In Vivo Mitochondrial Import. *Journal of Biological Chemistry*, *274*(18). https://doi.org/10.1074/jbc.274.18.12685

Opaliński, Ł., Song, J., Priesnitz, C., Wenz, L.-S., Oeljeklaus, S., Warscheid, B., Pfanner, N., & Becker, T. (2018). Recruitment of Cytosolic J-Proteins by TOM Receptors Promotes Mitochondrial Protein Biogenesis. *Cell Reports*, *25*(8). https://doi.org/10.1016/j.celrep.2018.10.083

Osellame, L. D., Blacker, T. S., & Duchen, M. R. (2012). Cellular and molecular mechanisms of mitochondrial function. *Best Practice & Research Clinical Endocrinology & Metabolism*, *26*(6), 711–723. https://doi.org/10.1016/j.beem.2012.05.003

Palmer, C. S., Anderson, A. J., & Stojanovski, D. (2021). Mitochondrial protein import dysfunction: mitochondrial disease, neurodegenerative disease and cancer. *FEBS Letters*, *595*(8). https://doi.org/10.1002/1873-3468.14022

Ponce-Rojas, J. C., Avendaño-Monsalve, M. C., Yañez-Falcón, A. R., Jaimes-Miranda, F., Garay, E., Torres-Quiroz, F., DeLuna, A., & Funes, S. (2017). αβ'-NAC cooperates with Sam37 to mediate early stages of mitochondrial protein import. *The FEBS Journal*, *284*(5). https://doi.org/10.1111/febs.14024

Reimann, B., Bradsher, J., Franke, J., Hartmann, E., Wiedmann, M., Prehn, S., & Wiedmann, B. (1999). Initial characterization of the nascent polypeptide-associated complex in yeast. *Yeast*, *15*(5). https://doi.org/10.1002/(SICI)1097-0061(19990330)15:5<397::AID-YEA384>3.0.CO;2-U

Schulz, C., Lytovchenko, O., Melin, J., Chacinska, A., Guiard, B., Neumann, P., Ficner, R., Jahn, O., Schmidt, B., & Rehling, P. (2011). Tim50's presequence receptor domain is essential for signal driven transport across the TIM23 complex. *Journal of Cell Biology*, *195*(4). https://doi.org/10.1083/jcb.201105098

Sen, A., & Cox, R. T. (2016). Clueless is a conserved ribonucleoprotein that binds the ribosome at the mitochondrial outer membrane. *Biology Open*, *5*(2). https://doi.org/10.1242/bio.015313

Sen, A., Kalvakuri, S., Bodmer, R., & Cox, R. T. (2015). Clueless, a protein required for mitochondrial function, interacts with the PINK1-Parkin complex in *Drosophila*. *Disease Models & Mechanisms*, *8*(6), 577–589. https://doi.org/10.1242/dmm.019208

Sharma, A., Mariappan, M., Appathurai, S., & Hegde, R. S. (2010). *In Vitro Dissection of Protein Translocation into the Mammalian Endoplasmic Reticulum* (pp. 339–363). https://doi.org/10.1007/978-1-60327-412-8_20

Sheffield, W. P., Shore, G. C., & Randall, S. K. (1990). Mitochondrial precursor protein. Effects of 70-kilodalton heat shock protein on polypeptide folding, aggregation, and import competence. *The Journal of Biological Chemistry*, *265*(19).

Sickmann, A., Reinders, J., Wagner, Y., Joppich, C., Zahedi, R., Meyer, H. E., Schonfisch, B., Perschil, I., Chacinska, A., Guiard, B., Rehling, P., Pfanner, N., & Meisinger, C. (2003). The proteome of Saccharomyces cerevisiae mitochondria. *Proceedings of the National Academy of Sciences*, *100*(23). https://doi.org/10.1073/pnas.2135385100

Suissa, M., & Schatz, G. (1982). Import of proteins into mitochondria. Translatable mRNAs for imported mitochondrial proteins are present in free as well as mitochondria-bound cytoplasmic polysomes. *Journal of Biological Chemistry*, *257*(21). https://doi.org/10.1016/S0021-9258(18)33620-2

Taylor, A. B., Smith, B. S., Kitada, S., Kojima, K., Miyaura, H., Otwinowski, Z., Ito, A., & Deisenhofer, J. (2001). Crystal Structures of Mitochondrial Processing Peptidase Reveal the Mode for Specific Cleavage of Import Signal Sequences. *Structure*, *9*(7). https://doi.org/10.1016/S0969-2126(01)00621-9

Terada, K., Ohtsuka, K., Imamoto, N., Yoneda, Y., & Mori, M. (1995). Role of heat shock cognate 70 protein in import of ornithine transcarbamylase precursor into mammalian mitochondria. *Molecular and Cellular Biology*, *15*(7). https://doi.org/10.1128/MCB.15.7.3708

Truscott, K. N., Kovermann, P., Geissler, A., Merlin, A., Meijer, M., Driessen, A. J. M., Rassow, J., Pfanner, N., & Wagner, R. (2001). A presequence- and voltage-sensitive channel of the mitochondrial preprotein translocase formed by Tim23. *Nature Structural Biology*, *8*(12). https://doi.org/10.1038/nsb726

Wegrzyn, R. D., Hofmann, D., Merz, F., Nikolay, R., Rauch, T., Graf, C., & Deuerling, E. (2006). A Conserved Motif Is Prerequisite for the Interaction of NAC with Ribosomal Protein L23 and Nascent Chains. *Journal of Biological Chemistry*, *281*(5). https://doi.org/10.1074/jbc.M511420200

Wiedmann, B., Sakai, H., Davis, T. A., & Wiedmann, M. (1994). A protein complex required for signal-sequence-specific sorting and translocation. *Nature*, *370*(6489), 434–440. https://doi.org/10.1038/370434a0

Williams, C. C., Jan, C. H., & Weissman, J. S. (2014). Targeting and plasticity of mitochondrial proteins revealed by proximity-specific ribosome profiling. *Science (New York, N.Y.)*, *346*(6210). https://doi.org/10.1126/science.1257522

Yamamoto, H., Esaki, M., Kanamori, T., Tamura, Y., Nishikawa, S., & Endo, T. (2002). Tim50 Is a Subunit of the TIM23 Complex that Links Protein Translocation across the Outer and Inner Mitochondrial Membranes. *Cell*, *111*(4). https://doi.org/10.1016/S0092-8674(02)01053-X

Yamamoto, H., Fukui, K., Takahashi, H., Kitamura, S., Shiota, T., Terao, K., Uchida, M., Esaki, M., Nishikawa, S., Yoshihisa, T., Yamano, K., & Endo, T. (2009). Roles of Tom70 in Import of Presequence-containing Mitochondrial Proteins. *Journal of Biological Chemistry*, *284*(46), 31635–31646. https://doi.org/10.1074/jbc.M109.041756

Young, J. C., Hoogenraad, N. J., & Hartl, F. U. (2003). Molecular chaperones Hsp90 and Hsp70 deliver preproteins to the mitochondrial import receptor Tom70. *Cell*, *112*(1). https://doi.org/10.1016/s0092-8674(02)01250-3